Aus dem Lehrstuhl Anatomie II – Neuroanatomie
Lehrstuhl der Ludwig-Maximilians-Universität München
Vorstand: Univ. Prof. Dr. med. Christoph Schmitz

Die Bedeutung des Tiergewichts und die Expression des G-Protein-gebundenen Rezeptors 17 (GPR17) bei Cuprizone-induzierter Demyelinisierung

Dissertation

zum Erwerb des Doktorgrades der Humanmedizin
an der Medizinischen Fakultät der
Ludwig-Maximilians-Universität zu München

vorgelegt von

Patrizia Maria Leopold
aus
Starnberg

2021

Mit der Genehmigung der Medizinischen Fakultät

der Universität München

Berichterstatter:	Prof. Dr. med. Dr. rer. nat. Markus Kipp
Mitberichterstatter:	Prof. Dr. med. Mikael Simons
	Prof. Dr. med. Uwe Ködel
Dekan:	Prof. Dr. med. dent. Reinhard Hickel
Tag der mündlichen Prüfung:	15.07.2021

Eidesstattliche Versicherung

Leopold, Patrizia Maria

Name, Vorname

Ich erkläre hiermit an Eides statt,
dass ich die vorliegende Dissertation mit dem Titel

Die Bedeutung des Tiergewichts und

die Expression des G-Protein-gebundenen Rezeptors 17 (GPR17)

bei Cuprizone-induzierter Demyelinisierung

selbstständig verfasst, mich außer der angegebenen keiner weiteren Hilfsmittel bedient und alle Erkenntnisse, die aus dem Schrifttum ganz oder annähernd übernommen sind, als solche kenntlich gemacht und nach ihrer Herkunft unter Bezeichnung der Fundstelle einzeln nachgewiesen habe.

Ich erkläre des Weiteren, dass die hier vorgelegte Dissertation nicht in gleicher oder in ähnlicher Form bei einer anderen Stelle zur Erlangung eines akademischen Grades eingereicht wurde.

München, 15.08.2021	Patrizia Maria Leopold
Ort, Datum	Unterschrift Doktorand

Inhaltsverzeichnis

1. Abkürzungsverzeichniss 5

2. Publikationsliste 6

2.1 Englischsprachige Orginalarbeiten 6

2.2. Posterpräsentation 6

3. Einleitung 7

3.1 Multiple Sklerose 7

3.2 Oligodendrozyten 9

3.3 Hirnläsionen 10

3.4 Pathomechanismen der Demyelinisierung und Remyelinisierung 11

3.5 G-Protein-gebundener Rezeptor 17 (GPR17) 12

3.6 Tiermodelle 13

3.7 Darstellung des Forschungsvorhabens 14

3.8 Eigenanteil an der Arbeit 16

4. Zusammenfassung 17

5. Summary 18

6. Veröffentlichung I 19

Nyamoya S, Leopold P, Becker B, Beyer C, Hustadt F, Schmitz C, Michel A, Kipp M: G-Protein-Coupled Receptor Gpr17 Expression in Two Multiple Sclerosis Remyelination Models. Molecular Neurobiology, 2019 19

7. Veröffentlichung II 35

Leopold P, Schmitz C, Kipp M: Animal Weight Is an Important Variable for Reliable Cuprizone-Induced Demyelination. Journal of molecular neuroscience, 2019 35

8. Literaturverzeichnis 43

9. Danksagung 46

1. Abkürzungsverzeichniss

bzw.	beziehungsweise
CC	Corpus Callosum
CD	[engl.] *cluster of differentiation*
DNS	Desoxyribonukleinsäure
EAE	Experimentelle autoimmune Enzephalomyelitis
engl.	englisch
GPR17	[engl.] *G-Protein-Coupled Receptor 17*, dt. G-Protein-gebundener Rezeptor 17
IBA1	[engl.] *Ionized Calcium-Binding Adapter Molecule one*
IF	Immunfluoreszenz
IHC	Immunhistochemie
KIS	klinisch isoliertes Syndrom
LFP	[engl.] *Luxol Fast Blue*
LPC	Lysophosphatidylcholin
MBP	[engl.] *myelin basic protein*
MRT	Magnetresonanztomographie
MS	Multiple Sklerose
mtDNS	mitochondriale Desoxyribonukleinsäure
OLIG2	Oligodendrozyten-Transkriptionsfaktor 2
OPC	[engl.] *oligodendrocyte progenitor cells*, dt. Oligodendrozyten Vorläuferzellen
PAS	[engl.] *Periodic Acid-Schiff Reaction*
PLP	Proteolipid-Protein
PPMS	primär-progrediente Multiple Sklerose
RRMS	schubförmig-remittierende Multiple Sklerose
rt RT-PCR	[engl.] *real time reverse transcription polymerase chain reaction*
SPMS	sekundär-progrediente Multiple Sklerose
ZNS	zentrales Nervensystem oder Zentralnervensystem

2. Publikationsliste

2.1 Englischsprachige Orginalarbeiten

Nyamoya S, **Leopold P**, Becker B, Beyer C, Hustadt F, Schmitz C, Michel A, Kipp M: G-Protein-Coupled Receptor Gpr17 Expression in Two Multiple Sclerosis Remyelination Models. Molecular Neurobiology, 2019. PMID: 29873041; DOI: 10.1007/s12035-018-1146-1

Leopold P, Schmitz C, Kipp M: Animal Weight Is an Important Variable for Reliable Cuprizone-Induced Demyelination. Journal of molecular neuroscience, 2019. PMID: 30937629; DOI: 10.1007/s12031-019-01312-0

Fischbach F, Nedelcu N, **Leopold P**, Zhan J, Clarner T, Nellessen L, Beißel C, van Heuvel Y, Goswami A, Weis J, Denecke B, Schmitz C, Hochstrasser T, Nyamoya S, Victor M, Beyer C, Kipp M: Cuprizone-induced graded oligodendrocyte vulnerability is regulated by the transcription factor DNA damage-inducible transcript 3. Glia, 2019. PMID: 30511355; DOI: 10.1002/glia.23538

2.2. Posterpräsentation

Leopold P, Nyamoya S, Kipp M: Demyelination, but not inflammation triggers oligodendrocyte progenitor activation. 113th Annual Meeting der Anatomischen Gesellschaft; 25. – 28. September 2018; Rostock, Germany

3. Einleitung

3.1 Multiple Sklerose

Die Multiple Sklerose (Enzephalomyelitis disseminata, MS) ist eine neurodegenerative und chronisch entzündliche Erkrankung des Zentralnervensystems (ZNS). Charakteristisch sind der Untergang von Oligodendrozyten, Demyelinisierung, Gliose, axonaler Schaden und die Rekrutierung und Aktivierung peripherer Immunzellen. Dies geschieht sowohl in der grauen wie auch in der weißen Substanz von Gehirn und Rückenmark und führt je nach Lokalisation zu unterschiedlichen fokalen neurologischen Ausfällen [1].

Weltweit sind mit einer Prävalenz von 30 pro 100 000 Personen mehr als zwei Millionen Menschen an MS erkrankt. Die ersten Symptome treten meist in der dritten oder vierten Lebensdekade auf, wodurch MS bei jungen Menschen den häufigsten Grund für neurologische Beeinträchtigungen darstellt. Die Ätiologie der Erkrankung ist noch nicht ausreichend geklärt. Derzeit wird von einer Kombination aus Umweltfaktoren und verschiedenen immunologischen und genetischen Einflussfaktoren ausgegangen. Frauen erkranken etwa doppelt bis dreifach so häufig wie Männer [2]. Beobachtungen zufolge haben Menschen in Europa oder Nordamerika im Vergleich zu äquatornäheren Regionen ein deutlich höheres Erkrankungsrisiko. Durch eine verminderte Sonnenlichtexposition wird weniger Vitamin D gebildet. Entsprechend verschiedener Studien wird das Risiko, an MS zu erkranken, durch einen erhöhten Vitamin-D-Spiegel im Blut gesenkt [3]. Weitere mögliche Prädilektionsfaktoren stellen beispielsweise Adipositas in jungen Jahren, Infektionen mit dem Epstein-Barr-Virus oder das Rauchen dar [4, 5].

Klinisch treten bei der MS vier Verlaufsformen auf: Zu Beginn der Erkrankung manifestiert sich häufig nur ein klinisch isoliertes Syndrom (KIS), welches auf eine fokale oder multifokale entzündliche Demyelinisierung schließen lässt, aber die Diagnosekriterien der MS noch nicht vollständig erfüllt [6, 7]. Typische Frühsymptome sind plötzliche Sehstörungen in Form einer unilateralen Optikusneuritis, Sensibilitätsstörungen oder Hirnstammsymptome wie beispielsweise Gangunsicherheiten [8]. Fisniku und Kollegen zeigten 2008, dass ein KIS in Kombination mit Gehirnläsionen in der Magnetresonanztomographie (MRT) das Risiko, im weiteren Verlauf an MS zu erkranken, um über 80 Prozent erhöht [9]. Die schubförmig-remittierende MS (RRMS) ist mit 85 bis 90 Prozent die häufigste Verlaufsform [8]. Ein Schub ist definiert als mindestens 24 Stunden andauerndes, neuaufgetretenes oder sich deutlich verschlechterndes Symptom ohne Nachweis von Fieber oder einer akuten Infektion. Patienten mit RRMS sind zwischen den Schüben neurologisch stabil und es kommt immer wieder zur Rückbildung der Schubsymptomatik [6]. Eine zu Beginn als RRMS diagnostizierte MS kann in eine sekundär-progrediente MS (SPMS) übergehen. Die Schübe treten bei diesen Patienten in der Regel nicht mehr auf und es kommt zu einer progredienten Verschlechterung der klinischen Symptomatik. Der Übergang ist im Regelfall schleichend. Bisher konnten keine klinischen, bildgebenden, immunologischen oder pathologischen Kriterien für eine Konversion zur SPMS gefunden werden [7]. Etwa 10 bis 15 Prozent der Patienten leiden von Beginn an unter einem progredienten, sich verschlechternden Verlauf

ohne Schübe. Diese Form der MS wird primär-progrediente Multiple Sklerose (PPMS) genannt. Diese Patienten sind bei Symptombeginn im Durchschnitt 10 Jahre älter als bei RRMS oder SPMS und die Geschlechterverteilung ist annähernd gleich [10]. Bei der PPMS scheint im Vergleich zur schubförmigen MS eine intakte Blut-Hirn-Schranke vorzuliegen. Die Invasion von Leukozyten durch die defekte Blut-Hirn-Schranke ist mit Merkmalen einer klassischen Autoimmunerkrankung vereinbar, während bei der PPMS eher von einer neurodegenerativen Erkrankung ausgegangen werden muss [11, 12].

Die MS zeigt je nach Ort der ZNS-Läsion ein sehr heterogenes Krankheitsbild. Die fokalneurologischen Defizite können beispielsweise Sensibilitätsstörungen, Sehstörungen, motorische Ausfälle, Gang-, Gleichgewichts- oder Koordinationsstörungen, Hirnstammsymptome, vegetative Funktionsstörungen und/oder psychische Störungen sein [5, 13]. Im klinischen Alltag wird der Krankheitsverlauf eines Patienten mit dem von John F. Kurtzke [14] entwickelten [engl.] *expanded disability status scale* (EDSS) bewertet. Die acht funktionellen Systeme (Pyramidenbahn, Kleinhirn, Hirnstamm, Sensorium, Blasen- und Mastdarmfunktion, Sehfunktion, zerebrale Funktion und sonstiges) und die Gehfähigkeit über 500 Meter werden getrennt voneinander evaluiert. In der Gesamtschau erhält der Patient einen Wert von null bis zehn, wobei null gesund und zehn dem Tod durch MS entspricht. Patienten mit einem Wert bis 4,5 sind über 500 Meter selbständig mobil, ab einem Wert von fünf nimmt die Einschränkung der Geh- und Bewegungsfähigkeit eine immer größere Rolle ein.

Die Diagnosefindung erfolgt in der Regel durch eine Kombination aus Anamnese, klinischen Symptomen, MRT Bildgebung, den Laborergebnissen der Liquorpunktion und gegebenenfalls einer elektrophysiologischen Untersuchung. Gehirnläsionen bei MS sind meist über drei Millimeter groß, asymmetrisch und treten überwiegend in der weißen, aber auch in der grauen Hirnsubstanz auf. Typische Lokalisationen sind periventrikulär, kortikal beziehungsweise (bzw.) juxtakortikal, infratentoriell, im Rückenmark und die Nervi optici. Aktive MS-Herde nehmen das Kontrastmittel Gadolinium auf und zeigen sich sowohl im T1 als auch im T2 gewichteten MRT hyperintens, während ältere MS-Herde nur in der T2 Sequenz hyperintens erscheinen [15]. Für die 2017 überarbeiteten McDonald-Diagnose-Kriterien der MS [6, 16] muss eine zeitliche und örtliche Dissemination der Läsionen vorliegen und die vorliegenden Befunde dürfen durch keine andere Erkrankung besser erklärt werden können. In der isoelektrischen Fokussierung des Liquors liegen bei über 90% der Patienten mit MS oligoklonale Banden vor [17]. Diese Banden entsprechen einer intrathekalen Immunglobulin-G-Synthese und können auch bei anderen akuten oder chronischen Entzündungen des ZNS auftreten. Bei einem neu aufgetretenen KIS verdoppeln oligoklonale Banden das Risiko für einen zukünftigen Schub [18]. Zur Unterstützung der Diagnosefindung oder als Verlaufsparameter können evozierte Potenziale mittels elektrophysiologischer Testung abgeleitet werden [19].

Eine frühe Diagnosestellung und somit ein früher Therapiebeginn sind ausschlaggebend für den weiteren Krankheitsverlauf. Die Behandlung der MS stützt sich nach den Leitlinien der

Deutschen Gesellschaft für Neurologie auf drei Säulen: die Behandlung der Erkrankungsschübe (Schubtherapie), die verlaufsmodifizierende Therapie mit Basis- und Eskalationstherapie und die Behandlung der MS-Symptome (symptomatische Therapie) [5]. Der akute MS-Schub wird mit einer Glukokortikosteroid-Stoßtherapie behandelt. Bei therapierefraktärer Schubsymptomatik trotz wiederholter hoch- bis ultrahochdosierter Glukokortikosteroid-Pulstherapie muss als Krisenintervention eine Plasmapherese bzw. Immunabsorption erwogen werden. Bei der schubförmigen MS und beim KIS werden als Basistherapie vorwiegend Interferon-beta-Präparate oder Glatirameracetat eingesetzt. Als Eskalationstherapie stehen bei diesen Patienten beispielsweise Fingolimod oder Natalizumab zur Verfügung. Neben Natalizumab wurden in den letzten Jahren mehrere therapeutische Antikörper, wie beispielsweise Rituximab, Alemtuzumab oder Ocrelizumab, für den Einsatz in der MS-Therapie zugelassen. Ocrelizumab hat beispielweise als eines der wenigen Therapeutika eine Zulassung für den Einsatz bei PPMS. Neben der Immunmodulation und Immunsuppression ist die symptomatische Therapie zur Verbesserung der Lebensqualität wichtiger Bestandteil der MS-Behandlung. Hierbei stehen vor allem Beschwerden wie Spastik, Ataxie, Tremor, Fatigue, kognitive Störungen, Blasenstörungen und sexuelle Dysfunktion im Vordergrund. Aktuell ist eine Heilung von MS nicht möglich [20].

3.2 Oligodendrozyten

Jean-Martin Charcot beschrieb bereits 1868 eine krankhafte Entzündung des Gewebes, welches die Nervenzellen umhüllt [21, 22]. Unter diesem Gewebe versteht man die Mark- oder Myelinscheide, die im ZNS von den Oligodendrozyten ausgebildet wird. Die Myelinscheiden stellen eine Art Isolationsschicht um die Axone dar, wodurch die Nervenleitgeschwindigkeit schneller und effizienter wird und die Axone mit Nährstoffen versorgt werden [23, 24].

Den embryonalen Ursprung der Oligodendrozyten stellen die Neuroepithelzellen dar. Diese entwickeln sich im Rahmen der Neuro- und Gliogenese weiter zu radialen Gliazellen, welche sich über intermediäre Vorläuferzellen zu Oligodendrozyten Vorläuferzellen, [engl.] *oligodendrocyte progenitor cells* (OPCs), Astrozyten oder Neuronen ausdifferenzieren [25]. Während ihrer Entwicklung verteilen sich die OPCs im gesamten ZNS [26] und differenzieren entweder zu myelinbildenden Oligodendrozyten aus oder persistieren im adulten Gehirn als residierende OPCs. OPCs sind im Gegensatz zu Oligodendrozyten in der Lage zur Zellproliferation und zur Gewebemigration und reagieren dementsprechend auf Gehirnschäden und Demyelinisierung [27]. Somit sind OPCs mit ihrer Möglichkeit zur Ausdifferenzierung zu myelinbildenden Oligodendrozyten ein wichtiger Ansatz für die Remyelinisierung und die Verhinderung von axonalem Schaden.

3.3 Hirnläsionen

Pathologische Merkmale der MS sind scharf begrenzte, fokal entzündliche Hirnläsionen mit Demyelinisierung, axonaler Degeneration und reaktiver Gliose. Diese Läsionen können sowohl in der weißen wie auch in der grauen Hirnsubstanz des gesamten ZNS auftreten. Histopathologisch lassen sich die MS-Läsionen nach Kuhlmann und Kollegen [28] in verschiedene Stadien einteilen.

Aktive Läsionen finden sich meist bei Patienten im frühen Krankheitsstadium. Charakterisiert sind sie durch eine hyperzelluläre Infiltration von Immunzellen, welche diffus über die gesamte Läsion verteilt sind. Makrophagen und Mikrogliazellen phagozytieren Myelin, sodass je nach Vorhandensein der Abbauprodukte in demyelinisierende und post-demyelinisierende aktive Läsionen unterschieden werden kann. Das frühe Stadium der aktiven demyelinisierenden Hirnläsionen wurde von Lucchinetti und Kollegen [29] in vier verschiedene Demyelinisierungs-Muster unterteilt: Muster I und II zeigen eine durch T-Lymphozyten und Makrophagen dominierte Entzündung. Bei Muster II zeigt sich außerdem eine deutliche Komplement- und Immunglobulin-Aktivierung. Beide Muster sind vorwiegend perivaskulär lokalisiert. Demyelinisierungs-Muster III ist durch Apoptose-typische, fragmentierte Oligodendrozyten mit kondensiertem Nukleolus charakterisiert. Bei Muster IV kommt es hingegen zu nicht-apoptotischer Degeneration der Oligodendrozyten mit Fragmentierung der Desoxyribonukleinsäure (DNS). Interessanterweise wies jede Autopsie ausschließlich ein für den Patienten typisches Demyelinisierungs-Muster auf.

Bei gemischt aktiv/inaktiven Läsionen liegt ein hypozelluläres Zentrum mit einem Randsaum aus Makrophagen und Mikrogliazellen vor. Die Läsionen sind bereits demyelinisiert und kommen vermehrt bei Patienten mit einem Krankheitsverlauf von über zehn Jahren vor.

Inaktive Läsionen sind hypozellulär, scharf begrenzt und fast komplett frei von reifen Oligodendrozyten. Eine ausgeprägte Degeneration der Axone kann neben dem nahezu vollständigen Myelinverlust beobachtet werden. Der Gewebeschaden wird in der Regel durch eine von Astrozyten gebildete Gliosenarbe ersetzt. In allen Stadien der Hirnläsionen kann es zur Remyelinisierung kommen. Diese ist häufig am Rand der Läsion lokalisiert und meist unvollständig ausgeprägt [28].

3.4 Pathomechanismen der Demyelinisierung und Remyelinisierung

Die chronisch-entzündliche Demyelinisierung sowie die neuronale Schädigung sind zentrale Merkmale der MS. Der genaue Pathomechanismus für den Gewebeuntergang ist jedoch noch nicht geklärt, wobei verschiedene Möglichkeiten/Prozesse diskutiert werden:

Durch eine Aktivierung autoreaktiver, peripherer, myelinspezifischer [engl.] *cluster of differentiation* (CD) 4^+ T-Lymphozyten und durch ein Zusammenspiel verschiedener Adhäsionsproteine und Liganden kommt es zur Durchwanderung der Blut-Hirn-Schranke, so dass diese T-Zellen in das zerebrale Parenchym eindringen. Dort werden die T-Lymphozyten durch [engl.] *myelin basic protein* (MBP) präsentierende Makrophagen und Mikrogliazellen erneut aktiviert und schütten proinflammatorische Zytokine aus, wodurch es zu einem weiteren Verlust der Blut-Hirn-Schranke und zu einer ausgeprägten Entzündungsreaktion mit Demyelinisierung kommt [30, 31]. Im entzündlichen Infiltrat von MS-Läsionen lassen sich außerdem zytotoxische $CD8^+$ T-Zellen finden. Diese können auf Oligodendrozyten direkt zytotoxisch wirken und deren Apoptose einleiten [32]. Neben den T-Zellen spielen autoreaktive B-Zellen eine wichtige Rolle in der Pathogenese der MS. Beispielsweise tragen sie durch die Bildung von Autoantikörpern gegen verschiedene Bestandteile von Myelin, Axonen und Neuronen und die Co-Stimulation von T-Zellen wesentlich zur Demyelinisierung und zur axonalen Schädigung bei [33].

Axonale Schädigung ist ein Hauptfaktor für Behinderungen bei MS. Bereits bei frühen Läsionen lässt sich ein deutlicher axonaler Schaden beobachten [34]. Bitsch und Kollegen zeigten, dass es unabhängig vom Grad der De- oder Remyelinisierung zu einer Schädigung der Axone in MS-Läsionen kommt. Das Ausmaß des axonalen Schadens korrelierte mit der Anzahl an Makrophagen, Mikrogliazellen und $CD8^+$ T-Lymphozyten, nicht aber mit der Anzahl der $CD4^+$ T-Lymphozyten und der Menge an den Entzündungsmediatoren Tumornekrosefaktor alpha und Nitrooxid. Somit ist davon auszugehen, dass die axonale Schädigung auch unabhängig von der Demyelinisierung abläuft und nicht nur als Konsequenz von dieser auftritt [35]. Allerdings ist das Ausmaß der axonalen Schädigung am höchsten in Läsionen mit starker Demyelinisierung und Mikroglia-Aktivierung [36]. Scheld und Kollegen konnten außerdem nachweisen, dass Neurodegeneration ein bedeutender Auslöser für die Rekrutierung von peripheren Immunzellen in das ZNS und somit für die Bildung von neuen, entzündlichen, demyelinisierten MS-Läsionen darstellt [37].

Ein weiterer Ansatz beschäftigt sich mit oxidativem Zell-Stress als zentrale Ursache der Demyelinisierung und des Gewebeuntergangs bei MS. In den Mitochondrien der Zellen findet an der Atmungskette die oxidative Phosphorylierung von ATP statt. Dieser Vorgang ist sauerstoffabhängig und dient zur Energiegewinnung. Sauerstoffradikale wie Stickstoffmonoxid blockieren kompetitiv die Bindung von Sauerstoff am vierten Komplex der Atmungskette, so dass es zu einer Fehlfunktion der Atmungskette kommt [38]. In MS-Läsionen konnten hochgradige Veränderungen an Komplexen der Atmungskette von Oligodendrozyten, Axonen und Astrozyten festgestellt werden [39]. Es ist außerdem bekannt, dass die mitochondriale DNS (mtDNS) sehr anfällig gegenüber Mutationen ist,

sodass es zu einer Akkumulation des mutierten mitochondrialen Genoms kommen kann [40]. Oligodendrozyten haben im Vergleich zu anderen Gliazellpopulationen schlechtere Reparaturmechanismen der mtDNS und sind anfälliger gegenüber oxidativem Stress und mtDNS Schaden [41]. Unter Stress stehende Oligodendrozyten sezernieren Chemokine und Zytokine wie Interleukin 6, die in die Signalkaskaden zur Aktivierung von Mikrogliazellen involviert sind [42]. An verschiedenen Stellen der normal erscheinenden weißen Hirnsubstanz von MS-Patienten werden apoptotische Oligodendrozyten, begleitet von einer starken Mikroglia-Aktivierung, beobachtet, während das Gewebe so gut wie frei von Lymphozyten und von myelinphagozytierenden Makrophagen ist. Demzufolge könnte die Apoptose von Oligodendrozyten der entzündlichen Demyelinisierung vorausgehen [43].

Zusammenfassend wird MS im Gegensatz zu früheren Annahmen nicht mehr als reine Autoimmunkrankheit angesehen, sondern man geht von einem dualen Konzept der Pathogenese aus. Einerseits kommen autoimmun-entzündliche und andererseits oxidative Prozesse als Grundlage einer initialen Demyelinisierung mit Neurodegeneration in Frage [1, 30].

Bei Autopsien kann in etwa 20 Prozent der MS-Läsionen eine deutliche Remyelinisierung nachgewiesen werden. Diese zeigt sich sowohl bei frühen wie auch bei älteren Hirnläsionen in allen Verlaufsformen und ist bei manchen Patienten stark ausgeprägt, während sie bei anderen fast gar nicht vorkommt [44]. Im Rahmen der Remyelinisierung kommt es zu einer Aktivierung und Proliferation von OPCs, Wanderung dieser OPCs in Richtung demyelinisiertes Axon und schließlich zu einer OPC-Axon-Interaktion mit Ausdifferenzierung der OPCs und Remyelinisierung. Der genaue molekularbiologische Mechanismus der Remyelinisierung und auch der Grund für die unzureichende Remyelinisierung bei der MS sind allerdings noch nicht abschließend geklärt [45].

3.5 G-Protein-gebundener Rezeptor 17 (GPR17)

Entsprechend vorangegangener Studien ist der G-Protein-gebundene Rezeptor 17 (GPR17) ein wichtiger Regulator in der Entwicklung und im Reifeprozess von Oligodendrozyten und der Remyelinisierung [46, 47]. In frühen Entwicklungsstadien der OPCs lässt sich nahezu keine Expression von GPR17 nachweisen. Beim Ausreifen der OPCs nimmt die GPR17-Expression kontinuierlich zu und erreicht ein Plateau in reifen Prä-Oligodendrozyten. Während der finalen Ausdifferenzierung ist die GPR17-Expression wieder rückläufig, bis sie in ausgereiften Oligodendrozyten nicht mehr nachweisbar ist. Die GPR17 Expression wird begleitet von der Expression spezifischer Prä-Oligodendrozyten-Marker-Proteine wie etwa von [engl.] *neural/glial antigen 2* (NG2), nicht aber von Markern für reife Oligodendrozyten wie z.B. Proteolipid-Protein (PLP) und MBP. Somit scheint GPR17 für den Beginn des Differenzierungsprozesses der OPCs notwendig, muss allerdings zur endgültigen Ausreifung der Oligodendrozyten und demzufolge zur Myelinisierung herunterreguliert werden. [48].

3.6 Tiermodelle

Verschiedene Tiermodelle stehen zur experimentellen Untersuchung der MS zur Verfügung, wobei keines der Modelle die MS in ihrer gesamten Komplexität darstellen kann. Vielmehr werden mit den verschiedenen Mausmodellen ausgewählte Versuche durchgeführt, um gezielte Pathomechanismen und Reparaturmechanismen der MS zu untersuchen [49].

Toxininduzierte Demyelinisierung mit anschließender Remyelinisierung kann entweder lokal durch eine Injektion oder durch systemische Gabe eines Toxins hervorgerufen werden. Für die lokale Injektion wird meistens Lysolecithin, auch Lysophosphatidylcholin (LPC) genannt, verwendet. LPC fungiert als Membrandetergent mit einer hohen Affinität zum MBP. Die Myelinscheiden werden abgebaut und innerhalb von wenigen Tagen kommt es in der betroffenen Region zur akuten Demyelinisierung [50, 51]. Remyelinisierung tritt in diesem Modell etwa zwei bis drei Wochen nach der Demyelinisierung auf [52, 53].

Für die systemische Intoxikation wird der Kupferchelator Cuprizone verwendet. Mitochondriale Enzyme der Atmungskette werden durch Cuprizone gehemmt, wodurch es zu oxidativem Zellstress kommt. Dieser führt zu primärer Oligodendrozytenapoptose mit begleitender Mikroglia- und Astrozyten-Aktivierung [1]. Die Behandlung mit Cuprizone führt bei Mäusen zu einer sehr gut reproduzierbaren Demyelinisierung von bestimmten Gehirnregionen. Unter diesen stellt das Corpus Callosum (CC) die am häufigsten untersuchte Region dar. Nach fünf bis sechs Wochen Cuprizone-Intoxikation ist das CC fast vollständig demyelinisiert, begleitet von massiver Mikrogliose, Astrogliose und axonalem Schaden. Dieses Verfahren wird akute Demyelinisierung genannt. Chronische Demyelinisierung kann durch eine verlängerte Cuprizonegabe über zwölf Wochen induziert werden. Bereits während der akuten Demyelinisierung kommt es zu einer Proliferation von OPCs, Migration in Richtung demyelinisierter Regionen und Ausdifferenzierung zu reifen Oligodendrozyten mit der Folge der Remyelinisierung. Wenn die Versuchstiere nach akuter Demyelinisierung wieder normales, Cuprizone-freies Futter erhalten, kann eine vollständige und schnelle Remyelinisierung beobachtet werden. Bei fortlaufender Cuprizone-Intoxikation oder nach chronischer Demyelinisierung ist die Remyelinisierung unzureichend oder bleibt komplett aus [49, 53].

Das Modell der experimentellen autoimmunen Enzephalitis (EAE) wird verwendet, um Entzündungen und autoimmunvermittelte Erkrankungen im ZNS zu untersuchen. Dieses ist im Gegensatz zu den toxininduzierten Modellen von einer T-Zell-Aktivierung und einem Zusammenbruch der Blut-Hirn-Schranke gekennzeichnet. Die Versuchstiere werden mit Myelinbestandteilen immunisiert, wodurch es zu einer t-zellvermittelten Immunantwort gegen das Myelin kommt. Die T-Lymphozyten dringen über die Blut-Hirn- und Blut-Liquor-Schranke in das Gehirn ein und lösen eine Entzündung im Rückenmark, im Kleinhirn und in den Nervi optici aus, während Großhirn, CC und subcortikale Strukturen weitgehend ausgespart bleiben. In den entzündeten Läsionen lässt sich neben blander Demyelinisierung ein akuter axonaler Schaden nachweisen [1, 54]. Die Remyelinisierung ist in diesem Mausmodell stark limitiert [53].

3.7 Darstellung des Forschungsvorhabens

Die meisten Behandlungskonzepte für die MS adressieren das Immunsystem und sind während der progressiven Phase der Erkrankung weniger effektiv oder sogar wirkungslos. Eine vielversprechende Strategie für neue MS-Medikamente ist daher der Schutz von Oligodendrozyten und die Verbesserung der Remyelinisierungsfähigkeit. Ein erster Schritt in Richtung promyelinisierender Therapie ist die Identifikation von Genen bzw. Proteinen, deren Expression während der De- und Remyelinisierung verändert ist.

Die erste Publikation charakterisiert detailliert die GPR17-Expression in weißen und grauen Hirnläsionen während experimenteller De- und Remyelinisierung. Die verwendeten Mausmodelle sind die klassischen Remyelinisierungsmodelle Cuprizone und LPC und zusätzlich das EAE-Modell. Die GPR17-Expression wurde auf Proteinebene mit Immunhistochemie (IHC) und Immunfluoreszenz (IF) und auf Ebene der Genexpression mit in-situ-Hybridisierung und [engl.] *real time reverse transcription polymerase chain reaction* (rt RT-PCR) analysiert. Nahezu alle GPR17-positiven Zellen exprimierten zusätzlich den Oligodendrozyten-spezifischen Oligodendrozyten-Transkriptionsfaktor 2 (OLIG2). Die Ergebnisse unserer Studie zeigen, dass die Induktion der GPR17-Expression mit akuter Demyelinisierung und endogener Remyelinisierung korreliert. Diese Induktion scheint allerdings zumindest im Cuprizone-Modell auf die weiße Gehirnsubstanz beschränkt. Gerade bei akuter Demyelinisierung ist dort eine starke Induktion der GPR17-Expression und ein vergleichsweise gutes Remyelinisierungspotenzial zu beobachten. Bei chronischer Demyelinisierung ist sowohl die Zahl der GPR17-positiven Zellen wie auch das Remyelinisierungspotenzial deutlich niedriger. Eine Modulation dieses Rezeptors und seiner Signalkaskade könnte somit eine mögliche therapeutische Konsequenz bei der Unterstützung der endogenen Remyelinisierung haben [45].

Grundlage eines Forschungsvorhabens an molekularbiologischen Mechanismen der Remyelinisierung im ZNS ist eine vorher stattgefundene und reproduzierbare Demyelinisierung. Die toxininduzierte Demyelinisierung beim Cuprizone-Mausmodell hat sich in der MS-Forschung für Studien mit Remyelinisierungsprozessen des ZNS etabliert [49, 53]. Neben der MS-Forschung wird das Neurotoxin Cuprizone für die Erforschung von Schizophrenie verwendet [55]. Neue Erkenntnisse und deren Studien müssen nachvollziehbar und auch für andere Labore wiederholbar sein. Somit ist der Wert des Modells abhängig von guten Protokollen, dem Wissen über alle seine quantifizierbaren Eigenschaften und einer genauen Kenntnis aller identifizierbaren Fehlerquellen und Störfaktoren. In vorangegangenen Studien wurden bereits wichtige Faktoren für eine reproduzierbare Cuprizone-induzierte Demyelinisierung identifiziert. Dabei handelt es sich unter anderem um das Geschlecht der Versuchstiere [56], ihre Geschlechtschromosomen [57], den genetischen Hintergrund [56] oder den Spiegel der zirkulierenden Sexualhormone [58]. Die Variable „Gewicht“ wurde bisher nie als einflussreicher Faktor für eine zuverlässige Demyelinisierung untersucht.

Die zweite Publikation beschäftigt sich aus diesem Grund mit dem Startgewicht der Versuchstiere als Einflussfaktor auf die durch Cuprizone vermittelte Demyelinisierung und die Reproduzierbarkeit der Ergebnisse. Hierfür prüften wir systematisch, ob eine Korrelation zwischen der Variablen „Gewicht am ersten Tag der Cuprizone-Intoxikation“ und den Variablen „Apoptose der Oligodendrozyten“, „Aktivierung von Mikrogliazellen“ und „Demyelinisierung“ besteht. Insgesamt wurden 21 Mäuse in die Studie eingeschlossen, wobei neun nach einer und zwölf nach drei Wochen Cuprizone-Intoxikation transkardial perfundiert wurden. Die Gehirnschnitte wurden anschließend histologisch untersucht. Nach einwöchiger Cuprizone-Intoxikation zeigte sich weder bei der Dichte der apoptotischen Zellen noch bei den [engl.] *Ionized Calcium-Binding Adapter Molecule one* (IBA1) -positiven Mikrogliazellen eine Korrelation mit dem Startgewicht. Des Weiteren konnten wir zu diesem Zeitpunkt keine Korrelation zu der Anzahl der OLIG2 exprimierenden Oligodendrozyten nachweisen. Die Cuprizone-Intoxikation scheint nach einer Woche unabhängig vom Startgewicht zu einer profunden Apoptose der Oligodendrozyten mit begleitender Mikroglia-Aktivierung zu führen. Histopathologisch werden erste Zeichen der Demyelinisierung nach drei Wochen Cuprizone-Intoxikation sichtbar. Durch [engl.] *Luxol Fast Blue* (LFB) und [engl.] *Periodic Acid-Schiff Reaction* (PAS) oder durch eine Färbung mit anti-PLP kann intaktes und beschädigtes Myelin visualisiert werden. Hier zeigte sich eine signifikant positive Korrelation zwischen dem Startgewicht der Versuchstiere und der anti-PLP Färbeintensität, sowie einen dazu parallelen, noch nicht signifikanten Trend bei der LFB/PAS Färbeintensität. In einem weiteren Versuch mit männlichen Mäusen konnte eine stark positive Korrelation zu der LFB/PAS Färbeintensität nachgewiesen werden. Zwischen dem Startgewicht und den IBA1-positiven Mikrogliazellen stellten wir in der manuellen Auszählung eine signifikant negative Korrelation und in der Densitometrie einen noch nicht signifikanten parallelen Trend fest. Somit ist nach drei Wochen Cuprizone-Intoxikation die zu beobachtende initiale Demyelinisierung und die Mikrogliazell-Aktivierung stärker, je niedriger das Startgewicht der Mäuse war. Die Studie zeigt nach unserem Wissen als erste, dass eine negative Korrelation zwischen dem Ausmaß der durch Cuprizone induzierten Demyelinisierung und dem Startgewicht der Tiere besteht. Demyelinisierung und Mikroglia-Aktivierung sind bei leichten Mäusen stärker als bei schweren Mäusen. Dies sollte in zukünftigen Studiendesigns berücksichtigt werden [59].

3.8 Eigenanteil an der Arbeit

Die vorliegende kumulative Dissertation umfasst zwei Publikationen.

Die erste Publikation (Nyamoya et al. G-Protein-Coupled Receptor GPR17 Expression in Two Multiple Sclerosis Remyelination Models. Molecular Neurobiology, 2018) stellt eine Zweitautorenschaft mit folgendem Arbeitsanteil dar:

- Literaturrecherche
- Immunhistochemie der Gehirnschnitte
- Datenerhebung und Auswertung
- Grafische Darstellung der Ergebnisse
- Abschlusskorrekturen

Die zweite Publikation (Leopold et al. Animal Weight Is an Important Variable for Reliable Cuprizone-Induced Demyelination. Journal of molecular neuroscience, 2019) stellt eine Erstautorenschaft mit folgendem Arbeitsanteil dar:

- Durchführung der Tierexperimente inklusive Cuprizone-Intoxikation, Käfigwechsel und Tötung der Tiere mittels kardialer Perfusion und Extraktion der Gehirne
- Literaturrecherche und Design der Studie
- Immunhistochemie der Gehirnschnitte
- Datenerhebung und Auswertung
- Grafische Darstellung und Ausarbeitung der Ergebnisse
- Abschlusskorrekturen und Revision

4. Zusammenfassung

Im Rahmen meiner wissenschaftlichen Arbeit beschäftigte ich mich mit Multiple Sklerose Mausmodellen.

Das Ziel der ersten Publikation war, die Expression des G-Protein-gebundenen Rezeptors 17 (GPR17) zu analysieren und diese in Relation zur De- und Remyelinisierung zu setzten. Wir verwendeten die toxininduzierten De- und Remyelinisierungsmodelle Cuprizone und LPC und das autoimmunvermittelte EAE-Model. GPR17 wird als ein wichtiger Regulator in der Entwicklung und im Reifeprozess von Oligodendrozyten verstanden. So exprimierten nahezu alle GPR17-positiven Zellen den spezifischen Oligodendrozyten-Marker OLIG2. Wir konnten zeigen, dass die GPR17-Expression mit akuter Demyelinisierung und suffizienter endogener Remyelinisierung korreliert. Zumindest im Cuprizone-Modell war diese auf die weiße Hirnsubstanz des Corpus Callosums beschränkt.

In der zweiten Publikation beschäftigten wir uns mit der Fragestellung, ob das Gewicht der Mäuse bei Beginn der Cuprizone-Intoxikation einen Einfluss auf eine zuverlässige und reproduzierbare Demyelinisierung hat. Hierzu untersuchten wir die Variablen „Apoptose der Oligodendrozyten“, „Aktivierung von Mikrogliazellen“ und „Demyelinisierung“. Nach einer Woche Cuprizone-Intoxikation war kein Einfluss des Startgewichtes erkennbar, während nach drei Wochen eine negative Korrelation zwischen den Variablen „Ausmaß der durch Cuprizone induzierten Demyelinisierung“ und „Startgewicht“ festgestellt wurde. Die Demyelinisierung und Mikroglia-Aktivierung waren in leichten Mäusen ausgeprägter als in schweren Mäusen.

Zusammenfassend wird in dieser Studie deutlich, dass in Tiermodellen auch bei vermeintlich unbedeutenden Parametern auf Homogenität innerhalb der Versuchstiere geachtet werden sollte, da es sonst zu einer Fehlinterpretation möglicher Ergebnisse kommen kann. Unsere Ergebnisse sind somit hoch relevant für das Design zukünftiger Studien mit dem Cuprizone-Tiermodell. Besonders durch dieses Modell konnten in der ersten wissenschaftlichen Arbeit neue Erkenntnisse über die Expression von GPR17 während der De- und Remyelinisierung gewonnen werden. Diese Daten untermauern das Interesse, zu evaluieren, ob die pharmakologische Modulation der GPR17-Signalkaskade den Remyelinisierungsprozess verbessern könnte.

5. Summary

Within the scope of my scientific work, I investigated multiple sclerosis mouse models.

The aim of the first publication was to analyze the expression of the G-protein-coupled receptor 17 (GPR17) and to relate it to de- and remyelination. We used the toxin-induced de- and remyelination models cuprizone and LPC and the autoimmune mediated EAE model. GPR17 is understood as an important regulator in the development and maturation process of oligodendrocytes. Almost all GPR17 positive cells expressed the specific oligodendrocyte marker OLIG2. We were able to show that GPR17 expression correlates with acute demyelination and sufficient endogenous remyelination. At least in the cuprizone model, this was limited to the white matter of the corpus callosum.

In the second publication we addressed the question of whether the weight of the mice at the onset of cuprizone intoxication has an influence on reliable and reproducible demyelination. For this, we examined the variables "oligodendrocytes apoptosis", "microglia activation" and "demyelination". After one week of cuprizone intoxication, no influence of the starting weight was detectable, while after three weeks a negative correlation between the variables "extent of cuprizone-induced demyelination" and "start weight" was found. Demyelination and microglia activation were more pronounced in low weight than in heavy weight mice.

In summary, this study clearly shows that in animal models, homogeneity within the experimental animals should be ensured even in the case of supposedly insignificant parameters, as otherwise a misinterpretation of possible results may occur. Our results are therefore highly relevant for the design of future studies using the cuprizone animal model. This model in particular enabled the first scientific study to gain new insights into the expression of GPR17 during de- and remyelination. These data support the interest in evaluationg wether A pharmacological modulation of the GPR17 signaling cascade to support the remyelination process would have to be evaluated in future studies.

6. Veröffentlichung I

Nyamoya S, Leopold P, Becker B, Beyer C, Hustadt F, Schmitz C, Michel A, Kipp M:

G-Protein-Coupled Receptor Gpr17 Expression

in Two Multiple Sclerosis Remyelination Models.

Molecular Neurobiology, 2019, Springer Nature

Molecular Neurobiology (2019) 56:1109–1123
https://doi.org/10.1007/s12035-018-1146-1

G-Protein-Coupled Receptor Gpr17 Expression in Two Multiple Sclerosis Remyelination Models

Stella Nyamoya[1,2] · Patrizia Leopold[2] · Birte Becker[1] · Cordian Beyer[1] · Fabian Hustadt[3] · Christoph Schmitz[2] · Anne Michel[3] · Markus Kipp[2]

Received: 22 January 2018 / Accepted: 22 May 2018 / Published online: 5 June 2018

Abstract

In multiple sclerosis patients, demyelination is prominent in both the white and gray matter. Chronic clinical deficits are known to result from acute or chronic injury to the myelin sheath and inadequate remyelination. The underlying molecular mechanisms of remyelination and its failure remain currently unclear. Recent studies have recognized G protein-coupled receptor 17 (GPR17) as an important regulator of oligodendrocyte development and remyelination. So far, the relevance of GPR17 for myelin repair was mainly tested in remyelinating white matter lesions. The relevance of GPR17 for gray matter remyelination as well as remyelination of chronic white matter lesions was not addressed so far. Here, we provide a detailed characterization of GPR17 expression during experimental de- and remyelination. Experimental lesions with robust and limited endogenous remyelination capacity were established by either acute or chronic cuprizone-induced demyelination. Furthermore, remyelinating lesions were induced by the focal injection of lysophosphatidylcholine (LPC) into the corpus callosum. GPR17 expression was analyzed by complementary techniques including immunohistochemistry, in situ hybridization, and real-time PCR. In control animals, GPR17$^+$ cells were evenly distributed in the corpus callosum and cortex and displayed a highly ramified morphology. Virtually all GPR17$^+$ cells also expressed the oligodendrocyte-specific transcription factor OLIG2. After acute cuprizone-induced demyelination, robust endogenous remyelination was evident in the white matter corpus callosum but not in the gray matter cortex. Endogenous callosal remyelination was paralleled by a robust induction of GPR17 expression which was absent in the gray matter cortex. Higher numbers of GPR17$^+$ cells were as well observed after LPC-induced focal white matter demyelination. In contrast, densities of GPR17$^+$ cells were comparable to control animals after chronic cuprizone-induced demyelination indicating quiescence of this cell population. Our findings demonstrate that GPR17 expression induction correlates with acute demyelination and sufficient endogenous remyelination. This strengthens the view that manipulation of this receptor might be a therapeutic opportunity to support endogenous remyelination.

Keywords CNS · Multiple sclerosis · Gpr17 · Cuprizone · LPC · Remyelination

Main Points
1. Cortical remyelination is delayed in the cuprizone model.
2. GPR17 expression is induced in the white but not gray matter.
3. GPR17 expression is induced in acute, but not chronic lesions.

Electronic supplementary material The online version of this article (https://doi.org/10.1007/s12035-018-1146-1) contains supplementary material, which is available to authorized users.

✉ Markus Kipp
markus.kipp@med.uni-muenchen.de

[1] Institute of Neuroanatomy and JARA-BRAIN, Faculty of Medicine, RWTH Aachen University, 52074 Aachen, Germany

[2] Department of Anatomy II, Ludwig-Maximilians-University of Munich, 80336 Munich, Germany

[3] Neurosciences TA Biology, UCB BioPharma, Braine L'Alleud, Brussels, Belgium

Introduction

Multiple sclerosis (MS) is an inflammatory disease of the central nervous system (CNS) associated with the development of large demyelinated plaques, oligodendrocyte destruction, and axonal degeneration. This pathology is paralleled by the activation of astrocytes and microglia as well as the recruitment of peripheral immune cells to the site of tissue injury. The feature, which distinguishes MS from other inflammatory and neurodegenerative disorders, is the formation of confluent plaques of primary demyelination. The sequence of molecular events leading to oligodendrocyte loss and consequently demyelination are not fully understood, but different stressors are known which can induce oligodendrocyte degeneration including oxidative stress, mitochondrial dysfunction, nitric oxide, protein misfolding, or inflammatory cytokine exposure [1, 2]. Of note, viable oligodendrocytes and an intact myelin sheath are indispensable for neuronal health. Oligodendrocytes provide nutritional support to neurons [3], fast axonal transport depends on oligodendrocytes [4], and mice deficient for mature myelin proteins display severe neurodegeneration [5].

Remyelination is one of the best-documented and most robust examples of tissue repair in the human adult CNS. Approximately 20–30% of postmortem MS tissues demonstrate remyelination, which can occur early and late during the course of the disease [6, 7]. Steps involved in this regenerative approach include activation and proliferation of oligodendrocyte progenitor cells (OPCs), migration of these OPCs towards the demyelinated axons, and OPC-axon interactions resulting in OPC differentiation and remyelination. Of note, the source of such OPCs might be manifold including progenitor cells dispersed in the brain parenchyma or located within neurogenic niches such as the subventricular zone [8]. Although the underlying mechanisms are poorly understood, remyelination is widespread in some MS patients, while in others it is sparse. A differentiation block of OPCs appears to be a major determinant of remyelination failure in chronic MS lesions [9]. Understanding why a relatively robust regenerative process should lose momentum is an important prerequisite for developing an effective therapeutic approach. Furthermore, while recent studies clearly showed that remyelination of the gray and white matter might be differentially regulated in both, MS [10] and its toxin-induced demyelination animal models [10–12], the underlying mechanisms are poorly understood.

Recent studies have recognized G protein-coupled receptors (GPCRs) as important regulators of oligodendrocyte development and maturation. At the most basic level, all GPCRs are characterized by the presence of seven membrane-spanning α-helical segments separated by alternating intracellular and extracellular loop regions. GPR17, in particular, is a G protein-coupled receptor that has been identified as regulator of remyelination [13–16]. Although the actual activating ligands for and some functions of this receptor are disputed, GPR17 has been reported to be activated by cysteinyl leukotrienes [17] and by purines such as ATP [18] or UDP [15]. GPR17 expression is almost absent in early OPCs, gradually increases in more mature precursors, reaches a plateau in immature/pre-oligodendrocytes, and then gradually decreases during terminal differentiation. In line with these findings, GPR17 is co-expressed with the early oligodendrocyte marker NG2 and markers of pre/immature oligodendrocyte phenotype but is downregulated in cells expressing myelin proteins such as myelin basic protein [18, 19]. It is, thus, believed that GPR17 is required for initiating the differentiation of OPCs but has to be downregulated to allow cells to undergo terminal maturation.

The consequence of GPR17 activation for oligodendrocyte differentiation and in consequence (re-)myelination appears to be context dependent. GPR17 transgenic mice with persistent GPR17 overexpression in specifically oligodendrocytes showed failure of proper developmental myelination, and in vitro *Gpr17* overexpression inhibited oligodendrocyte differentiation and maturation. Conversely, *Gpr17* knockout mice showed early onset of oligodendrocyte myelination suggesting that the loss of GPR17 function accelerates OPC differentiation and myelination [20]. In line with this finding, chemical activation of GPR17 inhibited the maturation of primary oligodendrocytes from heterozygous but not GPR17$^{-/-}$ mice in culture, as well as in cerebellar slices [21, 22], whereas inhibition of GPR17 activity with pranlukast promoted OPC differentiation in vitro. Beyond, the deletion of *Gpr17*, either globally or specifically in the oligodendrocyte lineage, resulted in an earlier onset of remyelination in a model of focally lysophosphatidylcholine-induced demyelination [13]. The hypothesis that deactivation of GPR17 is needed for oligodendrocyte maturation is further supported by the recent finding that GPR17 desensitization by G-protein receptor kinase phosphorylation and subsequent internalization are necessary events for terminal differentiation of OPCs [22]. Taken together, these data suggest that GPR17 acts to negatively regulate terminal oligodendrocyte differentiation and myelination. In contrast to these results, it has been reported that GPR17 activation by natural agonists can promote OPC differentiation in vitro [16, 19].

The most commonly used animal models used to study MS-related aspects of remyelination are toxin models. In principal, toxin-mediated demyelination with subsequent remyelination can be induced by either focal injection or systemic administration of the toxin. While focal demyelination is usually induced by injection of lysolecithin (also called lysophosphatidylcholine; LPC), the copper chelator cuprizone is used for systemic intoxication [23, 24]. LPC acts as a membrane detergent, resulting in rapid myelin sheath disassembly and, finally, demyelination in a matter

of days. In the cuprizone model, demyelination is due to a metabolic insult of oligodendrocytes. Cuprizone-induced primary oligodendrocyte apoptosis leads to almost complete demyelination in a matter of weeks (i.e., 5–6 weeks). In both models, endogenous remyelination is robust and occurs within weeks after induction of experimental demyelination [25, 26]. In contrast, endogenous remyelination is limited after prolonged cuprizone exposure (i.e., chronic demyelination) [24, 26].

In the current study, we aimed to analyze expression of GPR17 in different MS animal models and relate its expression to de- and remyelination.

Material and Methods

Animals

Seven- to 8-week-old C57BL/6 male and 8-week-old female mice were purchased from Janvier Labs, Le Genest-Saint-Isle, France. Microbiological monitoring was performed according to the Federation of European Laboratory Animal Science Associations recommendations. Animals were randomly allocated to the different experimental groups. A maximum of five animals were housed per cage (cage area 435 cm^2). Animals were kept under standard laboratory conditions (12 h light/dark cycle, controlled temperature 23 °C ± 2 °C and 55% ± 10% humidity) with access to food and water ad libitum. It was assured that researches and technicians did not use any light during the night cycle period. Nestlets were used for environmental enrichment. All cuprizone experiments were formally approved by Regierung Oberbayern (Bayern, Germany; reference number 55.2-154-2532-73-15). All lysophosphatidylcholine-induced experiments were performed according to the guidelines of the European Directive 2010/63/EU and Belgian legislation. The ethical committee for animal experimentation from UCB Biopharma SPRL (LA1220040 and LA2220363) approved the experimental protocols.

Induction of Experimental Demyelination

Systemic demyelination was induced by feeding male mice with ground standard rodent chow (Ssniff, Soest, Germany) containing 0.25% cuprizone [bis(cyclohexanone)oxaldihydrazone; Sigma-Aldrich Inc., St Louis, MO, USA] for the indicated treatment period. Control groups were fed standard rodent chow. In summary, 71 mice were used for the cuprizone experiments.

Focal demyelination was induced by stereotactic injection of the membrane detergent lysophosphatidylcholine (LPC; $n = 9$). All surgical procedures were performed under general anesthesia by intraperitoneal injections of ketamine (50 mg/kg body weight; Nimatek, Eurovet Animal Health B.V.) and medetomidine (0.5 mg/kg body weight; Domitor Orion Corporation). Mice recovery was accelerated with one injection of 2.5 mg/kg atipamezole (Antisedan, Orion Corporation). In order to prevent dehydration, mice were subcutaneously injected with 500 μL of Ringer's solution (B. Braun, Germany). For the stereotactic surgery, mice were fixed in a standard stereotaxic frame (model 900 and mouse adaptor model 922; Kopf CA, USA). The scalp was incised, and two drill holes were made at the following coordinates relative to the bregma to target the corpus callosum in both hemispheres: anterior-posterior − 1.10 mm, medial-lateral ± 0.90 mm, and dorsal-ventral − 1.45 from the skull (mm) [27, 28]. A 1% LPC solution (two administrations of 0.75 μL of 10 μg/μL LPC from bovine brain; Ref L1381, Cas Number 9008-30-4, Sigma-Aldrich; Germany in saline) was injected with a syringe needle (1702 (25 μL), 33 gauges, 8 mm length; Hamilton, Bonaduz, Switzerland), protected from light with aluminum, and connected to a syringe pump (Model Legato 130, KD Scientific), at a flow rate of 0.2 μL/min. Control animals ($n = 10$) received 0.75 μL of saline as a vehicle solution instead. To ensure complete diffusion and avoid spillage into neighboring structures, the needle was left in place for 2.5 min before being slowly retracted. The animals were monitored daily after surgery and finalized after 5 days by transcardial perfusion.

Induction of experimental autoimmune encephalomyelitis (EAE) in female mice was induced by injection of an emulsion of $MOG_{35–55}$ peptide dissolved in complete Freund's adjuvant followed by injection of pertussis toxin in PBS according to the manufacturer's recommendations (Hooke Laboratories, USA). Disease severity was scored as published previously [29]. The animals were monitored daily and finalized 14 days after immunization (i.e., at peak of the disease).

Tissue Preparation

For histological and immunohistochemical studies (IHC), preparation of tissues was performed as previously described [30]. In brief, mice were transcardially perfused with ice-cold PBS followed by a 3.7% paraformaldehyde solution (PFA; pH 7.4). After overnight post-fixation in the same fixative, the brains were dissected and embedded in paraffin, and coronal or medio-sagittal 5-μm-thick sections were prepared for immunohistochemistry or in situ hybridization. The spinal cords were incubated in EDTA (ethylenediaminetetraacetic acid) for 48 h at 37 °C (changed once) prior to paraffin embedding. Coronal slices were analyzed at the level 265 (i.e., ventral hippocampus) according to the mouse brain atlas published by Sidman et al. (http://www.hms.harvard.edu/research/brain/atlas.html). For gene expression studies, mice were transcardially perfused with ice-cold PBS and corpus callosum, cortex, and spinal cord tissues were manually

dissected and snap-frozen in liquid nitrogen. Samples were then kept at − 80 °C until further processing.

Immunohistochemistry (IHC) and (Densitometric) Analysis

For immunohistochemistry, sections were rehydrated and, if necessary, antigens were unmasked with heating in Tris/EDTA (pH 9.0) or citrate (pH 6.0) buffer. After washing in PBS, sections were incubated overnight (4 °C) with anti-proteo-lipid antibodies to detect myelin ([PLP] 1:5000), or with anti-G protein-coupled receptor 17 antibodies to detect pre-myelinating oligodendrocytes ([GPR17] 1:200). The next day, slides were incubated either with biotinylated secondary antibodies [(i) horse anti-mouse IgG, 1:50; (ii) goat anti-rabbit IgG, 1:50] for 1 h and then with peroxidase-coupled avidin–biotin complex (ABC-HRP kit; order number PK-6100, RRID AB 2336819, Vector Laboratories, Burlingame, USA) and treated with 3,3′-diaminobenzidine (order number K3468, DAKO, Hamburg, Germany) as a peroxidase substrate. Some slides were incubated with the EnVision System-HRP Labeled Polymer [(iii) goat anti-mouse; (iv) goat anti-rabbit]. A detailed list of applied antibodies are given in Table 1 and Table 2.

Stained and processed sections were digitalized using a Nikon Eclipse 80i microscope (Nikon, Nikon Instruments, Germany) equipped with a DS-2MV camera. The open source program ImageJ 1.48v (NIH, Bethesda, MD, USA) was used to evaluate staining intensity using semi-automated densitometrical evaluation after threshold setting. In brief, acquired images were converted to gray scale images, and a global thresholding algorithm was used for dividing each image into two classes of pixels (black and white, i.e., binary conversion). Global thresholding works by choosing a value cutoff, such that every pixel less than that value is considered one class, while every pixel greater than that value is considered the other class. Relative staining intensity was then quantified in binary converted images, and results are presented as percentage area.

Stained sections of a different cohort of mice were additionally scanned using the Nikon Eclipse E200 microscope (Nikon Instruments, Germany) equipped with a Basler acA1920-40um camera (Basler AG, Ahrensburg, Germany) and a manual scanning software (manualWSI software, Microvisioneer, München, Germany). Cell numbers were quantified after manually delineating the region of interest (ROI) using the program ViewPoint (PreciPoint GmbH, Freising, Germany).

Luxol Fast Blue (LFB) Periodic Acid–Schiff (PAS) Stain

For validation of the myelination data, intact and damaged myelin was additionally visualized using LFB/PAS histochemical stains. To this end, slides were deparaffinized in 4 × 5 min xylene, rinsed 3 × 3 min in 100% ethanol, followed by 2 × 5 min in 96% ethanol. Sections were then subsequently incubated in LFB solution (0.1 g Luxol fast blue (order number 7709, Carl Roth, Germany) in 100 mL 96% ethanol plus 500 μL acetic acid (order number 3738, Carl Roth, Germany), overnight at 60 °C. On the next day, sections were dipped in 96% followed by water and processed in a lithium carbonate solution (0.05 g lithium carbonate [order number 1.05680.0250, Merck, Germany] in 100 mL aqua dist.). Sections were further differentiated in 70% ethanol for a few seconds and rinsed in water. Afterwards, oxidation was performed in periodic acid (0.5 g periodic acid [order number 1.00524.0025, Merck, Germany] in 100 mL aqua dist.). Sections were rinsed followed by incubation in Schiff's reaction (order number 1.09033.0500, Merck, Germany) for 15 min, then rinsed in warm tap water for 5 min and counterstained with hematoxylin (order number 1.04302.0025, Merck, Germany) for 1 min. Sections were dehydrated and subsequently mounted in Depex (order number 18243, Serva, Germany) for further analyses.

Immunofluorescence Double Labeling

For immunofluorescence double labeling, sections were rehydrated, unmasked with Tris/EDTA buffer (pH 9.0) and heating, blocked with PBS containing 2% heat-inactivated fetal calf serum ([FCS], order number A15-152, PAA, Germany) and 1% bovine serum albumin ([BSA], order number 0163, Carl Roth, Germany), and incubated overnight (4 °C) with the combination of primary antibodies diluted in blocking solution. Anti-GPR17 (1:100) was either combined with anti-OLIG2 (1:1000) to visualize oligodendrocytes, with

Table 1 Primary antibodies used in this study

	Order number	RRID	Supplier
GFAP	ab10062	AB 296804	abcam, UK
GPR17	10136	AB 10613826	Cayman chemicals, Michigan, USA
NeuN	MAB377	AB 2298772	Millipore, Germany
OLIG2	MABN50	AB 10807410	Millipore, Germany
PDGFRα	ab51875	AB 870652	abcam, UK
PLP	MCA839G	AB 2237198	Biorad, Puchheim, Germany

Table 2 Secondary antibodies used in this study

	Order number	RRID	Supplier
Horse anti-mouse IgG	BA-2000	AB 2313581	Vector Laboratories, Burlingame, USA
Goat anti-rabbit IgG	BA-1000	AB 2313606	Vector Laboratories, Burlingame, USA
Alexa Fluor 488 goat IgG anti-rabbit	A11008	AB 143165	Invitrogen, USA
Alexa Fluor 546 goat IgG anti-rabbit	A11010	AB 2534077	Invitrogen, USA
Alexa Fluor 546 goat IgG anti-mouse	A21133	AB 2535772	Invitrogen, USA
Alexa Fluor 488 donkey IgG anti-mouse	A21202	AB 141607	Invitrogen, USA
Alexa Fluor 488 donkey IgG anti-mouse	A21208	AB 2535794	Invitrogen, USA
EnVision System- HRP Labeled Polymer goat anti-rabbit	K4003	AB 2630375	DAKO, Hamburg, Germany
EnVision System-HRP Labeled Polymer goat anti-mouse	K4001		DAKO, Hamburg, Germany

anti-GFAP (1:1000) to visualize astrocytes, with anti-PDGF receptor alpha (1:100) to visualize oligodendrocyte progenitor cells, or with anti-NeuN (1:2000) to visualize neurons. After washing, sections were incubated in a combination of fluorescent anti-rabbit secondary antibodies (1:500, Alexa Fluor) and fluorescent anti-mouse secondary antibodies (1:500, Alexa Fluor), or fluorescent anti-rat secondary antibodies (1:500, Alexa Fluor) both diluted in blocking solution. Subsequently, sections were incubated with Hoechst 33342 solution (1:10000, order number H3570, Life Technologies, USA) diluted in PBS for the staining of cell nuclei. A detailed list of applied antibodies is given in Table 1 and Table 2.

To rule out unspecific binding of the fluorescent secondary antibodies to primary antibodies, appropriate negative controls were performed by first incubating sections with the primary antibodies and subsequently incubating these sections with switched fluorescent secondary antibody. Unspecific secondary antibody binding to the tissue itself was checked by performing negative controls by incubating sections with each of the fluorescent secondary antibodies alone (data not shown). Stained and processed sections were documented with the Leica microscope DMI6000B (Leica Microsystems, Germany). Cell numbers were quantified after manually delineating the corpus callosum using the open source program ImageJ 1.48v (NIH, Bethesda, MD, USA). For a clearer demonstration, colors were digitally adjusted using ImageJ, in order to use an identical color code in the representative figures.

In Situ Hybridization

A commercial fluorescence in situ hybridization kit (ViewRNA® in situ hybridization tissue assay, Affymetrix-Panomics, order number QVT0012) was used for single labeling of formalin-fixed, paraffin-embedded tissues, according to the manufacturer's recommendations. Protease digestion time was adjusted to 20 min. The probe for *Gpr17* was purchased from Affymetrix (Affymetrix-Panomics, VB1-13617 Type 1). Fluorescence images were captured using the Leica microscope DMI6000B (Leica Microsystems), and cell numbers were quantified using open source program ImageJ 1.48v (NIH, Bethesda, MD, USA) after manually outlining the corpus callosum.

Gene Expression Analyses

Gene expression levels were analyzed using cDNA from the isolated tissues, with real-time reverse transcription-PCR (Bio-Rad, Germany) using SensiMix SYBR and Fluorescein (Bioline, Germany). Primer sequences and individual annealing temperatures are shown in Table 3. Results were normalized to ß-actin as the reference gene and target gene expression was calculated using the ΔΔCt method. Melting curves were analyzed and PCR products were routinely separated by gel electrophoresis to determine the specificity of the PCR reaction (data not shown).

Statistical Analysis

Statistical analyses were performed using Prism 5 (GraphPad Software Inc., San Diego, CA, USA). All data are given as arithmetic means ± SEMs. A p value of ≤ 0.05 was considered to be statistically significant. Applied statistical tests are given in the respective figure legends. Normal distribution was assumed. No outliers were excluded from the analyses.

Results

In the cuprizone model, demyelination is robust after a 5-week intoxication period. After termination of intoxication, endogenous remyelination occurs and is complete within 3 to 4 weeks. In a first step, we investigated changes of

Table 3 Sequence of primers used in this study

	Sense	Antisense	bp	AT
Gpr17	GCT TAC TCT GAG CAA TGC GGA	GTG ATA AAC CAA CCG GGT AGG	222	62
ß-actin	GTA CCA CCA TGT ACC CAG GC	AAC GCA GCT CAG TAA CAG TCC	247	60

Gpr17 expression during acute demyelination and early remyelination. To this end, one cohort of mice was sacrificed after 5 weeks cuprizone intoxication, whereas another was sacrificed after 7 days recovery and compared to control animals (see Fig. 1 (A) for the experimental setup of this part of the study). *Gpr17* mRNA expression levels were analyzed by rt RT-PCR and in situ hybridization, whereas GPR17 protein expression was investigated by immunohistochemistry. To verify de- and remyelination, respectively, mid-sagittal sections were processed for anti-PLP immunohistochemistry. Anatomical landmarks in the mid-sagittal plane are shown in Fig. 1 (B). As demonstrated in Fig. 1 (C, C'), profound demyelination of the medial (mCC) and caudal (cCC) part of the corpus callosum was readily visible after 5 weeks cuprizone intoxication. Demyelination was as well present within the rostral part of the corpus callosum (rCC), even though loss of anti-PLP staining was incomplete there. In line with previous reports [31], demyelination was as well extensive in the gray matter cortex (see star in Fig. 1 (C)). Other regions were resistant to the 5 weeks cuprizone intoxication period such as the anterior commissure (ac), or diverse midbrain structures (mid). After 7 days of recovery, semi-maximal remyelination was evident in the previously demyelinated structures. While pronounced recovery of anti-PLP staining loss was evident in the caudal corpus

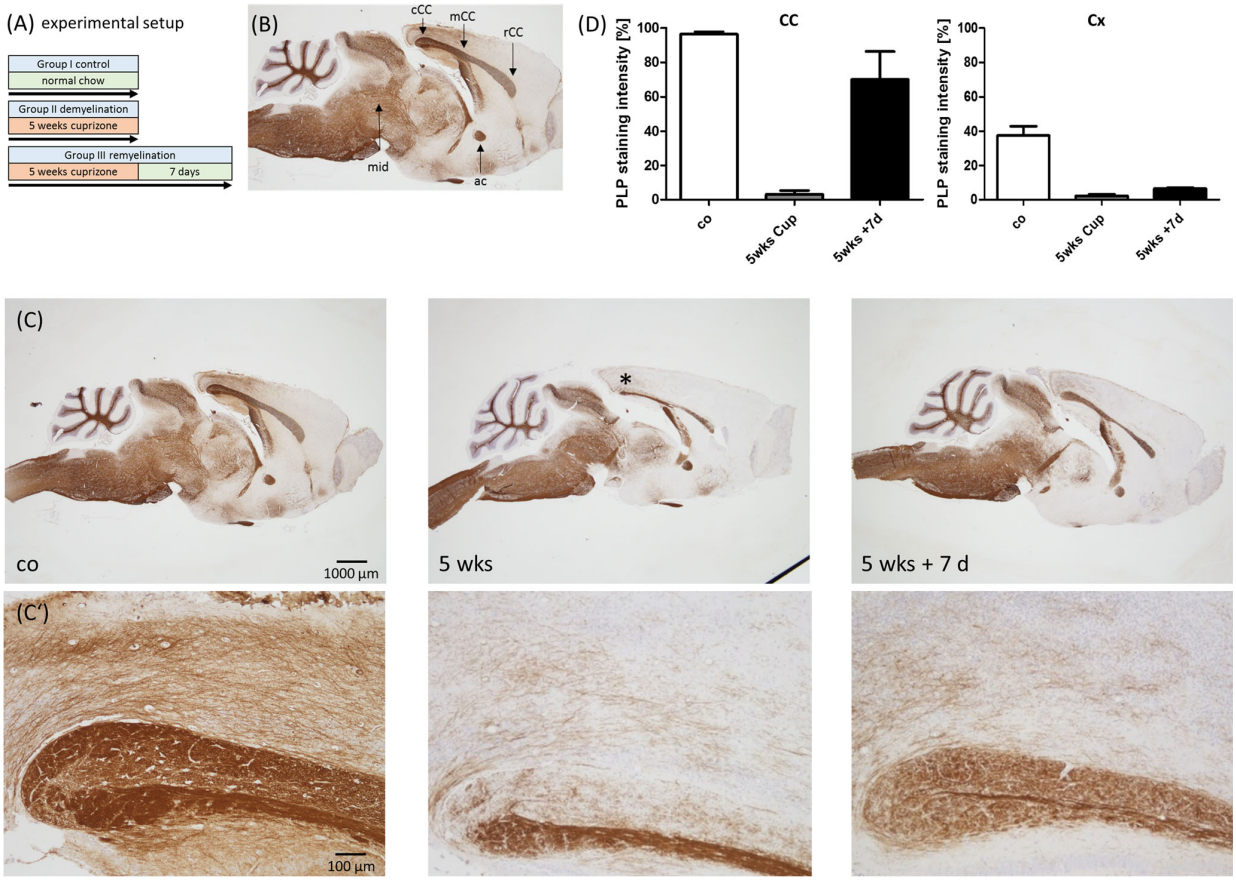

Fig. 1 Cuprizone-induced de- and remyelination. (A) Schematic depicting the experimental setup. Group I was sacrificed after 5 weeks normal chow (control), group II after acute demyelination (5 weeks cuprizone; 0.25%), and group III after early remyelination (5 weeks cuprizone, followed by 7 days recovery). (B) Anatomical landmarks in the mid-sagittal plane: cCC caudal corpus callosum, mCC medial corpus callosum, rCC rostral corpus callosum, mid midbrain, ac anterior commissure. (C, C') Expression of PLP, visualized by anti-PLP immunohistochemistry. (D) Quantification of anti-PLP staining intensity by densitometric analysis (two biological replicates each). Note the severe demyelination of the caudal and medial corpus callosum and gray matter cortex (star in C). As well, note the ongoing remyelination in the CC, but not in the cortex region

callosum (co 96.39 ± 1.37%; 5 weeks 3.005 ± 2.325%; 5 weeks + 7 days 70.02 ± 16.36%), recovery of anti-PLP staining intensity was minor in the gray matter cortex (co 37.4 ± 5.49%; 5 weeks 2.235 ± 0.925%; 5 weeks + 7 days 6.38 ± 0.63%) (see Fig. 1 (D)). Demyelination and early remyelination of the corpus callosum was as well observed in LFB/PAS-stained sections (data not shown).

Next, we aimed to correlate de- and remyelination with GPR17 expression. Anti-GPR17 immunohistochemistry in control animals revealed numerous GPR17$^+$ cells evenly distributed within the white matter corpus callosum and gray matter cortex. Especially in the cortex, GPR17$^+$ cells displayed a multipolar morphology with multiple, fine-branched processes, reminiscent of pre-myelinating oligodendrocytes (see insert in Fig. 2 (A)). In the white matter corpus callosum, GPR17$^+$ cells as well displayed fine processes; however, these appeared to be aligned in parallel to axonal fiber bundles. After 5 weeks cuprizone intoxication, a profound accumulation of GPR17$^+$ cells was found, especially in the rostral and caudal part of the corpus callosum (arrows), less so in its medial portion (see Fig. 2 (B)). This accumulation persisted during the recovery period (see Fig. 2 (C)). Densitometric evaluation revealed increased anti-GPR17 staining intensity in the corpus callosum of cuprizone-treated mice (co 18.12 ± 3.015%; 5 weeks 81.16 ± 5.77%; 5 weeks + 7 days 74.71 ± 9.2%). In contrast, GPR17 staining intensity was not increased in the demyelinated and remyelinating cortex (co 72.54 ± 26.99%; 5 weeks 49.39 ± 23.37%; 5 weeks + 7 days 84.98 ± 8.17%) (see Fig. 2 (D)). For a more detailed analysis, we quantified numbers of GPR17$^+$ cells in the gray matter cortex. As shown in Fig. 2 (E), numbers of GPR17$^+$ cells slightly decreased after 5 weeks cuprizone intoxication (co 19.5 ± 1.5 cells/mm^2; 5 weeks 14.5 ± 2.5 cells/mm^2) and remained at this reduced level after 7 days remyelination (5 weeks + 7 days 15.5 ± 2.5 cells/mm^2). Since GPR17 expression in oligodendrocyte progenitor cells has been shown to be down-regulated during terminal oligodendrocyte differentiation [19], an additional cohort of mice was analyzed after a 11-day remyelination period. As demonstrated in Fig. 2 (F, G), numerous GPR17$^+$ cells were found in the corpus callosum at week 5, but numbers were significantly lower after prolonged remyelination. Comparable to our observation at day 7, while there was sufficient remyelination of the white matter corpus callosum, remyelination of the gray matter cortex was delayed at day 11.

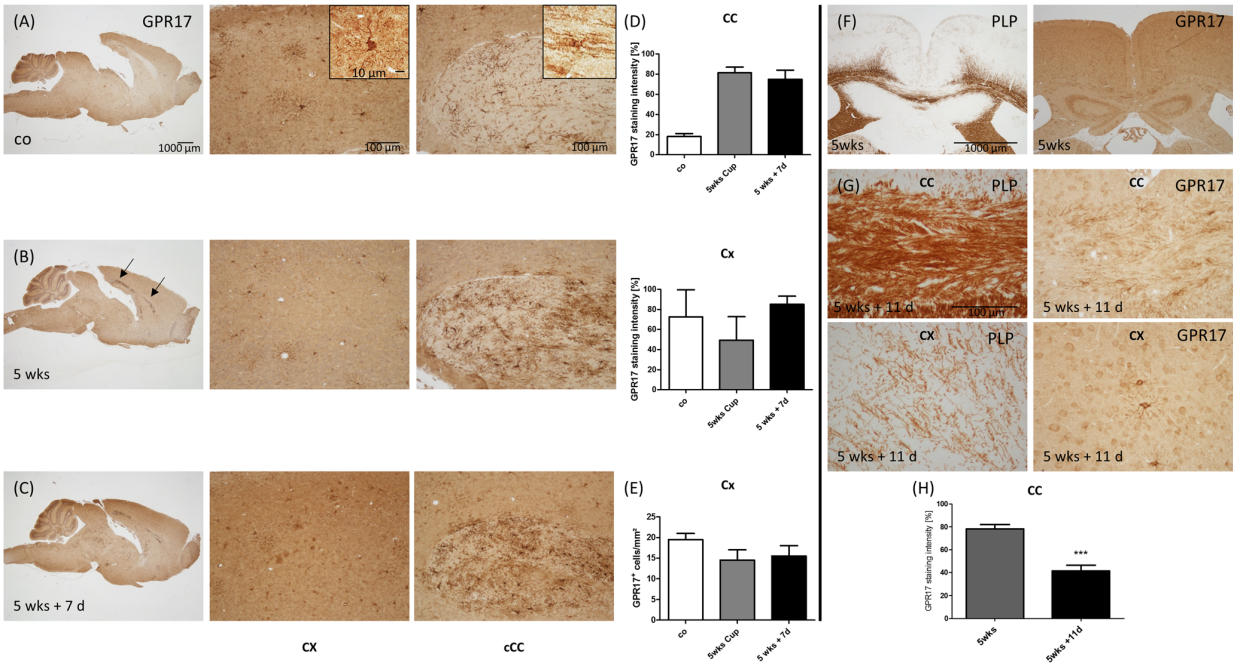

Fig. 2 Cuprizone-induced demyelination leads to GPR17$^+$ cell accumulation in the corpus callosum but not in the cortex region. Expression of GPR17, visualized by anti-GPR17 immunohistochemistry, in control (A), 5 weeks (B), and 5 weeks cuprizone, followed by 7 days recovery groups (C, sagittal plane). Inserts in the upper row depict the morphology of a gray and white matter GPR17$^+$ cell, respectively. (D) Quantification of anti-GPR17 staining intensity by densitometric analysis in the white matter corpus callosum and gray matter cortex (two biological replicates). (E) Quantification of GPR17$^+$ cell numbers in the gray matter cortex (two biological replicates). Note the induction of GPR17 in the corpus callosum, but not in the cortex region. (F, G) Representative anti-PLP and anti-GPR17 immunohistochemistry of the midline of the corpus callosum (coronal plane) after 5 weeks cuprizone (F) and 5 weeks cuprizone followed by 11 days recovery (G). (H) Quantification of anti-GPR17 staining intensity by densitometric analysis in the white matter corpus callosum (at least six biological replicates each). CC corpus callosum, Cx cortex. Differences between groups were statistically tested using a two-tailed *t* test; ***$p \leq 0.001$

To verify our results obtained on the protein level, *Gpr17* mRNA expression was additionally analyzed in a parallel cohort of mice. As shown in Fig. 3 (A), rt RT-PCR analysis with isolated corpus callosum tissues revealed *Gpr17* expression induction after 5 weeks cuprizone intoxication (co 100 ± 19.57% vs 5 weeks 611.3 ± 180.6%). Increased *Gpr17* mRNA expression levels remained stable during the 7 days recovery period (5 weeks + 7 days 526.2 ± 251.4%). Minor expression induction was as well found in isolated cortex tissues (co 100 ± 11.14%; 5 weeks 147 ± 21.57%; 5 weeks + 7 days 120.7 ± 8.719%); however, this induction failed to reach statistical significant levels. In line with these observations, higher numbers of $Gpr17^+$ cells were as well observed in the corpus callosum by in situ hybridization (co 76 ± 27.77 cells/mm^2; 5 weeks 254.5 ± 88.15 cells/mm^2; 5 weeks + 7 days 190.5 ± 17.32 cells/mm^2) (see Fig. 3 (B, C)). To verify that GPR17$^+$ cells belong to the oligodendrocyte lineage, sections were processed for OLIG2/GPR17, GFAP/GPR17, and NeuN/GPR17 immunofluorescence double labeling (see Fig. 4). As shown in Fig. 4 (A), and in line with our results presented above, densities of OLIG2$^+$/GPR17$^+$ cells (yellow) were low (34 ± 1 cells/mm^2) in control animals, but high at week 5 (142 ± 9 cells/mm^2) and after 7 days of remyelination (137.5 ± 28.5 cells/mm^2). Densities of OLIG2$^+$/GPR17$^-$ cells (red) were higher compared to the OLIG2$^+$/GPR17$^+$ cell population, most likely representing OLIG2$^+$ mature oligodendrocytes (co 1203 ± 118 cells/mm^2; 5 weeks 623.5 ± 119.5 cells/mm^2; 5 weeks + 7 days 1318 ± 183 cells/mm^2). Of note, OLIG2$^-$/GPR17$^+$ cells (green) were virtually absent at all investigated time points (co 3 ± 3 cells/mm^2; 5 weeks 7.5 ± 7.5 cells/mm^2; 5 weeks + 7 days 1.5 ± 1.5). In line with these findings, almost no GFAP$^+$/GPR17$^+$ cells were found in the corpus callosum of control and cuprizone-intoxicated mice (see Fig. 4 (B)). Double labeling experiments for NeuN and GPR17 showed that some cells in the cortex stained positive for both antigens (see Fig. 4 (C)). Of note, none of these GPR17/NeuN double-positive cells displayed the characteristic morphology of OPCs.

Next, we investigated at what time point GPR17 expression induction occurs in the cuprizone model. To this end, another cohort of mice was fed cuprizone for up to 5 weeks, processed at different time points for immunohistochemistry, and compared to control animals. As shown in Fig. 5 (A), a profound demyelination of the medial part of the corpus callosum was readily visible after 5 weeks cuprizone intoxication. Demyelination was not evident at week 1 or 3. Densitometric evaluation of the anti-GPR17 staining intensity revealed a significant increase of GPR17 expression in the corpus callosum at week 5 (co 31.76 ± 5.392% vs 5 weeks 80.92 ± 8.332%; $p \leq 0.001$) (see Fig. 5 (C)). In line with this finding, a significant higher number of GPR17$^+$ cells were found in the corpus callosum (co 45.98 ± 3.517 cells/mm^2 vs 5 weeks 205.4 ± 33.62 cells/mm^2; $p \leq 0.001$) but not in the cortex region (co 21.28 ± 1.829 cells/mm^2 vs 5 weeks 25.23 ± 1.368 cells/mm^2) after 5 weeks cuprizone intoxication (Fig. 5 (D, E)).

Next, we were interested whether induction of GPR17 expression is restricted to the cuprizone model, or is as well

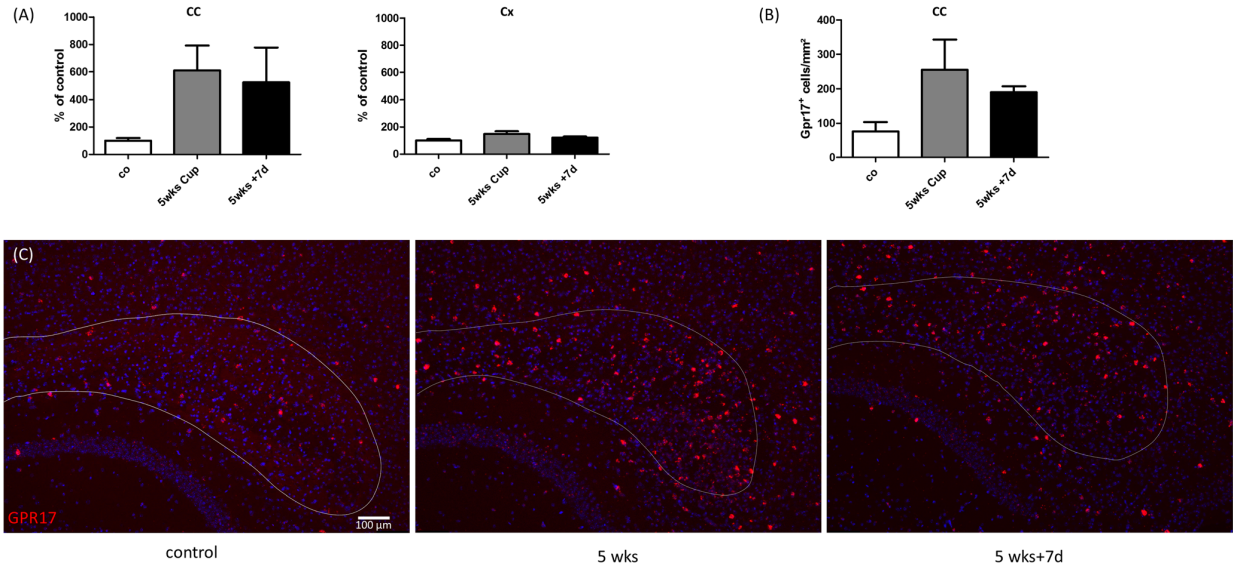

Fig. 3 Cuprizone-induced demyelination induces Gpr17 mRNA expression in the corpus callosum but not in the cortex region. (A) *Gpr17* mRNA expression in the isolated corpus callosum of control, 5 weeks cuprizone, and 5 weeks cuprizone followed by 7 days recovery groups (at least three biological replicates). Differences between groups were statistically tested using one-way ANOVA with the obtained *p* values corrected for multiple testing using Dunnett's post hoc. (B) Quantification of *Gpr17*$^+$ cell numbers in the corpus callosum visualized by in situ hybridization (two biological replicates). (C) Representative images of *Gpr17* in situ hybridization experiments in the mid-sagittal plane. Dotted line, border of the caudal corpus callosum; blue, Hoechst; red, *Gpr17*

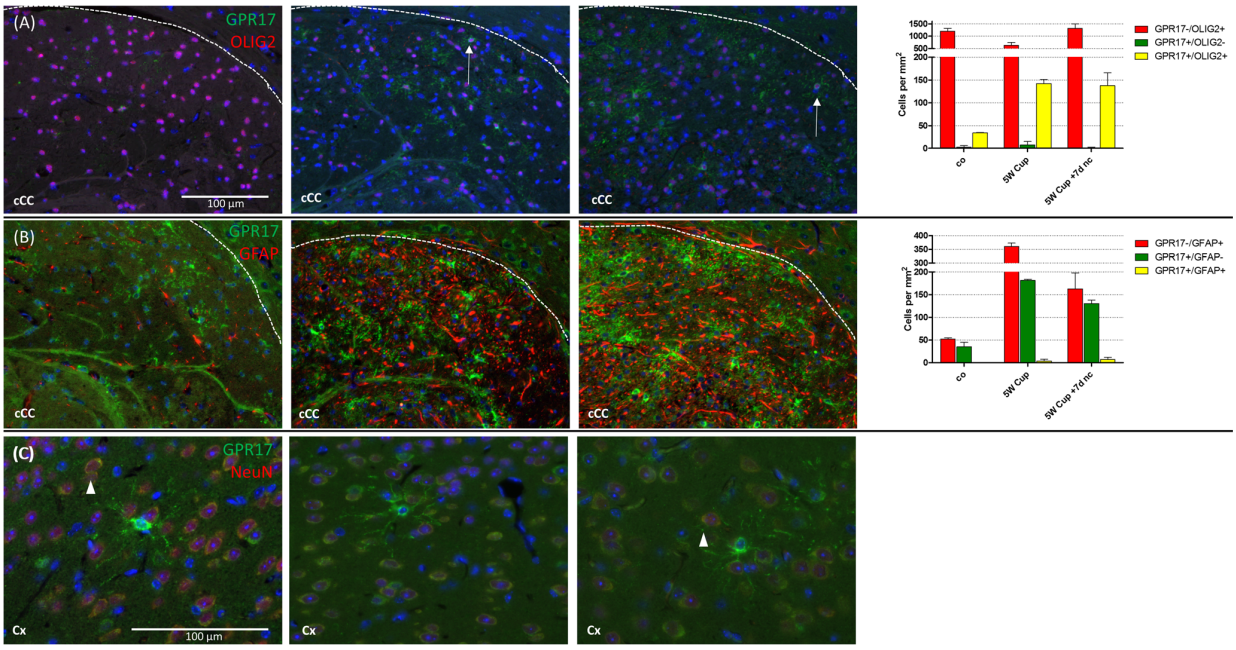

Fig. 4 GPR17$^+$ cells belong to the oligodendrocyte lineage. Representative double immunofluorescence stains of the caudal corpus callosum of control, 5 weeks cuprizone, and 5 weeks cuprizone followed by 7 days recovery groups (left side) and quantification of distinct cell populations (right side; two biological replicates each). The dotted line delineates the border of the caudal corpus callosum towards the neocortex; white arrows highlight GPR17$^+$ cells expressing as well OLIG2. Green, GPR17; red, OLIG2 (A), GFAP (B), NeuN (C); blue, Hoechst. Note that virtually all GPR17$^+$ cells as well express the oligodendrocyte marker protein OLIG2 (A). Almost no GPR17$^+$ cells express the astrocytic GFAP marker protein (B). Further, note that some neocortical NeuN$^+$ neurons express GPR17 (see arrowheads)

evident in another model of experimental demyelination with robust remyelination. To this end, we induced focal demyelination by stereotactic injection of the membrane detergent lysophosphatidylcholine (LPC) into the corpus callosum [32, 33]. Five days after bilateral lesion induction (indicated by orange lines in Fig. 6 (A)) with either vehicle or LPC, brains were processed for immunohistochemistry. As shown in Fig. 6 (A), LFB/PAS stains revealed profound demyelination of the midline of the caudal corpus callosum in LPC-injected (stars) but not vehicle-injected mice (co 99.4 ± 0.4% vs LPC 4.333 ± 0.333%; $p \leq 0.001$) (see Fig. 6 (C)). Vehicle-injected mice showed small GPR17$^+$ cells with thin and ramified processes (see Fig. 6 (B)). Densitometric quantification of GPR17 staining intensity revealed a highly significant increase of GPR17 expression within the LPC-injected compared to the vehicle-injected corpus callosum (co 9.208 ± 1.063% vs LPC 39.28 ± 3.769%; $p \leq 0.001$) (see Fig. 6 (B)).

Next, we wanted to investigate GPR17 expression in an experimental setting with limited endogenous remyelination capacity. To this end, a separate cohort of animals was intoxicated with cuprizone for 5 weeks (i.e., acute demyelination) or 12 weeks (i.e., chronic demyelination), and numbers of GPR17 cells were quantified in the midline of the corpus callosum and compared to control animals. As demonstrated in Fig. 7 (A), severe demyelination was evident at weeks 5 and 12. In line with our previous findings, numbers of GPR17$^+$ cells in the corpus callosum were significantly increased after a 5-week cuprizone intoxication period (co 44 ± 9.597 vs 5 weeks 245 ± 16.66 cells/mm^2; $p \leq 0.001$). The number of GPR17$^+$ cells was low after chronic cuprizone-induced demyelination (12 weeks 68.80 ± 2.107 cells/mm^2). To clarify if low GPR17 expression in chronic lesions is due to loss of OPCs, subsequent sections were stained for the OPC marker protein platelet-derived growth factor receptor alpha (PDGFRα). As demonstrated in Fig. 7 (C), densities of PDGFRα-expressing cells were low in control animals, high after acute, and intermediate after chronic cuprizone-induced demyelination, respectively. Statistical comparison revealed significant lower densities of PDGFRα$^+$ cells after chronic (112.2 ± 34.35 cells/mm^2) compared to acute demyelination (340 ± 37.07 cells/mm^2; $p \leq 0.01$).

Finally, we wanted to investigate GPR17 expression in an autoimmune model of MS, namely, experimental autoimmune encephalomyelitis (EAE). As demonstrated in Fig. 8, in both spinal cord sections of control and EAE mice, GPR17$^+$ cells what appeared to be motoneurons were found in the ventral horn (see arrowheads in Fig. 8 (C, G)). Similar to what we found in the forebrain, GPR17$^+$ cells with a multipolar morphology and multiple, fine-branched processes were found in the gray and white matter spinal cord (see arrowhead in Fig. 8

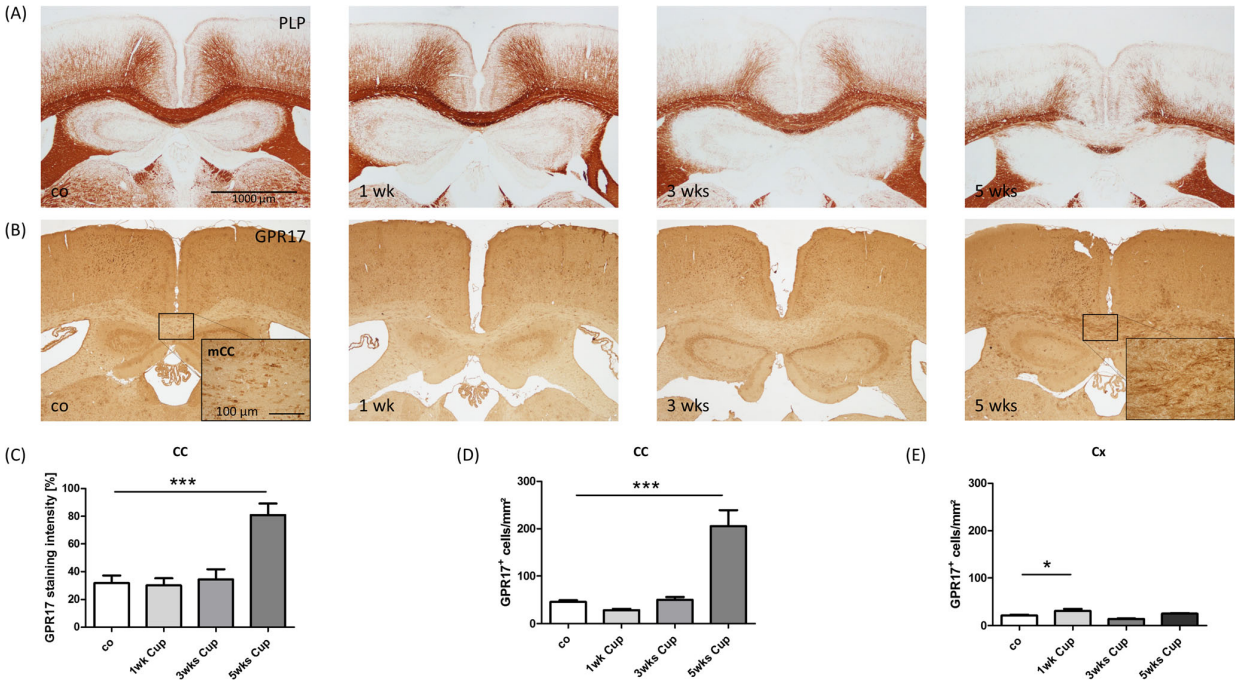

Fig. 5 GPR17 induction in the course of cuprizone-induced demyelination. (A) Representative anti-PLP stains of control mice and mice intoxicated with cuprizone for 1, 3, and 5 weeks. (B) Representative anti-GRP17 stains of control mice and mice intoxicated with cuprizone for 1, 3, and 5 weeks. High-power views show the midline of the corpus callosum (mCC). (C) Quantification of anti-GPR17 staining intensity by densitometric analysis in the white matter corpus callosum (at least four biological replicates). (D) Quantification of GPR17$^+$ cell numbers in the corpus callosum (at least four biological replicates). (E) Quantification of GPR17$^+$ cell numbers in the cortex (at least four biological replicates). Differences between groups were statistically tested using one-way ANOVA with the obtained p values corrected for multiple testing using Dunnett's post hoc test; *$p \leq 0.05$ or ***$p \leq 0.001$

(D)). It appeared that the densities of such GPR17$^+$, small, ramified cells was higher in inflammatory white matter spinal cord lesions of EAE mice; however, no induction of *Gpr17* mRNA expression was observed by rt RT-PCR in a separate cohort of animals (co 100 ± 18.04%; EAE 81.57 ± 10.05%; data not shown).

Discussion

Because most therapeutic strategies for MS target the immune system and are less effective or even ineffective in the progressive phase of the disease, preservation of oligodendrocytes or increasing their remyelinating capacity is a promising strategy for novel MS treatments. A first step towards developing potential promyelinating therapies is to identify genes whose expression is affected during demyelination and subsequent remyelination. In this study, we used two commonly applied remyelination models, namely, the cuprizone and the LPC model, to study expression of the G-protein-coupled receptor Gpr17 on the mRNA and protein level. GPR17 was previously found to be expressed in OPCs and premature oligodendrocytes [19], and it has been proposed to have a role in OPC differentiation and developmental myelination [14, 20, 34]. These studies showed that GPR17 inhibits OPC differentiation in vitro and delays myelination during development in vivo. Furthermore, GPR17 activation inhibited oligodendrocyte survival in the LPC model [13]. The same authors showed that inhibition of GPR17 promoted oligodendrocyte differentiation and remyelination. Pharmacological inhibition of GPR17 could, therefore, be considered as a potential therapeutic approach for enhancing myelin repair.

In a first step, we investigated the expression of GPR17 in the cuprizone model. After 5 to 6 weeks of cuprizone intoxication, specific parts of the corpus callosum are almost completely demyelinated, a process called "acute demyelination." Acute demyelination is followed by spontaneous remyelination during subsequent weeks when mice are fed normal chow. In contrast, endogenous remyelination is highly restricted when cuprizone administration is prolonged (12 weeks or longer), a process called "chronic demyelination" [24, 26]. In line with the results from other groups, our immunohistochemical stains using anti-GPR17 antibodies showed that GPR17$^+$ cells are present in similar numbers in the white matter, corpus callosum, and gray matter cortex [35]. Consistent with previous reports, by immunohistochemistry, we observed two distinct cortical GPR17$^+$ cell populations: first, non-neuronal cells labeled with single

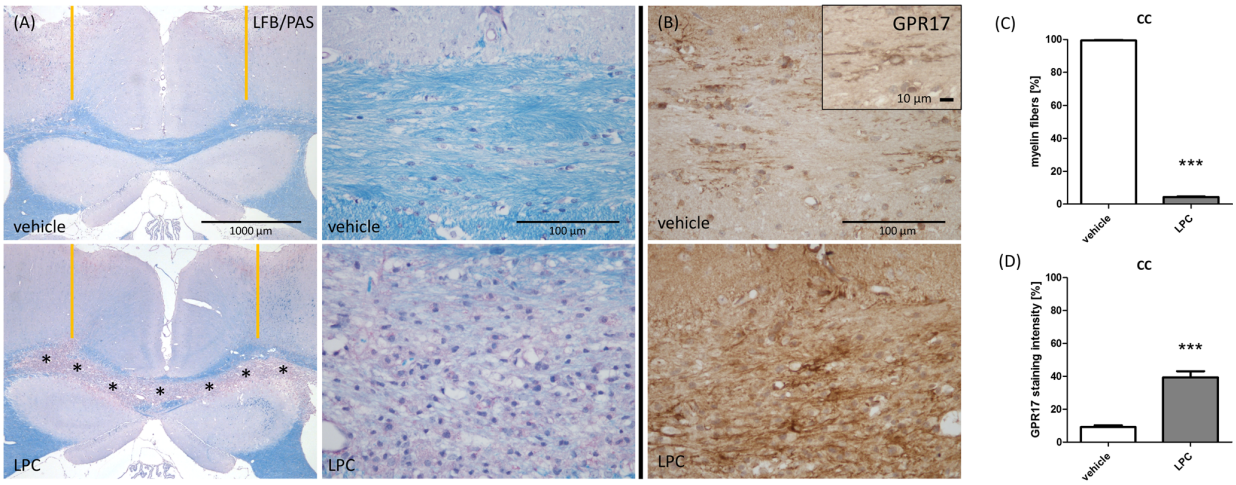

Fig. 6 Focal demyelination leads to GPR17$^+$ cell accumulation. (A) Representative LFB/PAS staining of vehicle (upper row) or LPC-injected (lower row) mice. The orange lines illustrate the theoretical position of the needles during the bilateral stereotactic LPC injection. The midline of the corpus callosum is shown on the right in higher magnification. Note the complete demyelination of the midline of the corpus callosum (stars and high-power view). (B) Expression of GPR17 in vehicle (upper picture) and LPC-injected (lower picture) mice, visualized by anti- GPR17 immunohistochemistry. (C) Quantification of LFB/PAS staining intensity by blinded evaluation of the white matter corpus callosum (at least nine biological replicates). (D) Quantification of anti-GPR17 staining intensity by densitometric analysis in the white matter corpus callosum (at least nine biological replicates). Differences between groups were statistically tested using unpaired *t* test; ***$p \leq 0.001$. Note the intense accumulation of GPR17-expressing cells in the demyelinated corpus callosum

intracellular spots or a staining on the whole cell membrane. These cells were characterized by a small, heavily stained cell soma and a network of highly branched cellular processes. The processes extended into all directions with no obvious preferential spatial orientation. Although not formally proven in this study, we propose that these GPR17$^+$ cells resemble NG2-glia [34]. Second, we observed faintly stained GPR17$^+$ cells what appeared to be (pyramidal) neurons. Expression of GPR17 in neocortical neurons was further verified by immunofluorescence double labeling experiments using anti-NeuN antibodies (see Fig. 4). Beyond, cells what appeared to be spinal cord motoneurons strongly expressed GPR17 (see Fig. 8). Whether or not such observed neuronal staining pattern are specific remains to be clarified in future studies. In this context, a recent study should be mentioned demonstrating that GPR17 can drive the fate of neural precursor cells by instructing precursors towards the neuronal lineage [36]. That the applied antibody principally is valid was verified by our follow-up gene expression studies: both in situ *hybridization* and rt RT-PCR analyses verified *Gpr17* expression induction in the demyelinated corpus callosum. It is tempting to speculate about the potential function of these stellate GPR17$^+$ cells. The morphology is somewhat reminiscent of resting, ramified microglia cells [37]. With their highly branched processes and protrusions, microglial cells continuously screen the extracellular space in a seemingly random fashion and at a high turnover rate [38]. A similar function might fulfill GPR17$^+$ OPC. With their highly developed network of cellular processes, GPR17$^+$ OPC might survey their environment for a potential demyelinating insult to initiate OPC activation, proliferation, and finally remyelination. In fact, it has been suggested that GPR17 may act as a "sensor" that is activated upon brain injury and may play a key role in orchestrating local remodeling/repair responses [16]. In an elegant study, Vigano and colleagues were able to show, by using a GPR17-iCreER(T2) mouse line for fate mapping studies, that virtually all GPR17 expressing cells co-express the oligodendrocyte-specific transcription factor OLIG2. No GFP$^+$ neurons, astrocytes, or microglia were detected [34]. Comparably, we observed that almost all GPR17$^+$ cells are OLIG2$^+$ and do not express GFAP. GPR17-expressing cells therefore most likely resemble adult OPCs. Due to their comparable densities in the white matter corpus callosum and gray matter cortex region, the potential for endogenous remyelination of both areas should be comparable.

In this context, it is interesting to note that the expression of GPR17 is induced in the white matter corpus callosum, but not in the gray matter cortex after experimental demyelination. Our data are in line with the findings from another cuprizone study showing accumulation of NG2$^+$ cells in the corpus callosum but not in the cortex [39]. The same group demonstrated a lower remyelination potential of the cortex compared to the white matter corpus callosum [11].

But why should cortical remyelination be less effective or slower, respectively? Using the cuprizone model, it has recently been shown that the temporal dynamics of OPC differentiation varies significantly between white and gray matter regions. While OPCs rapidly repopulate the corpus callosum and mature into myelinating oligodendrocytes, OPC differentiation in the gray matter occurs much more

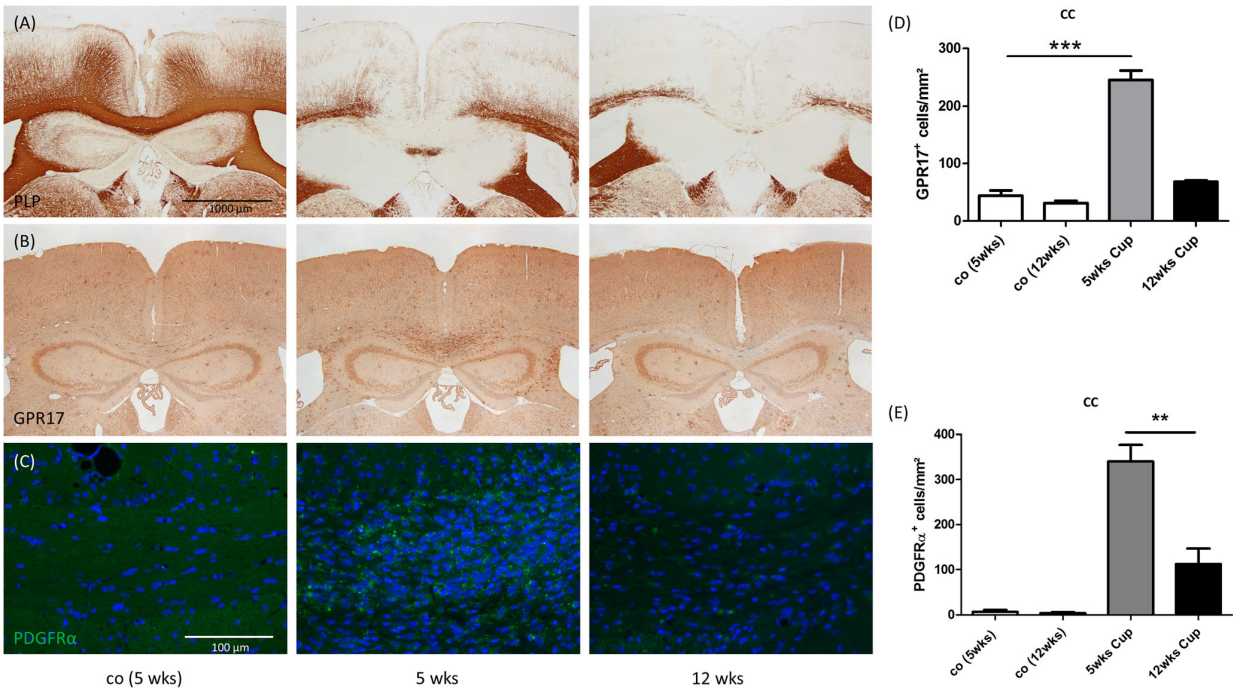

Fig. 7 GPR17 expression in acute and chronic cuprizone lesions. Representative anti-PLP (A), anti-GPR17 (B), and anti-PDGFRα stains of control mice and mice intoxicated with cuprizone for 5 or 12 weeks. (D) Quantification of GPR17$^+$ cell numbers in the white matter corpus callosum (five biological replicates each). Differences between groups were statistically tested using one-way ANOVA with the obtained p values corrected for multiple testing using Dunnett's post hoc test; $^{***}p \leq 0.001$. (E) Quantification of PDGFRα$^+$ cell numbers in the white matter corpus callosum (five biological replicates each). Differences between groups (5 and 12 weeks) were statistically tested using unpaired t test; $^{**}p \leq 0.01$

slowly, resulting in a delay in remyelination relative to the corpus callosum [12]. Xing and colleagues were recently able to show that in cuprizone-challenged mice, substantial numbers of neural precursor cells migrate into the demyelinated corpus callosum and, there, contribute to oligodendrogenesis [8]. Delay of cortical remyelination might, therefore, simply be due to a failure of neural precursor cells to migrate the long distance from the subventricular zone into the cortex. To what

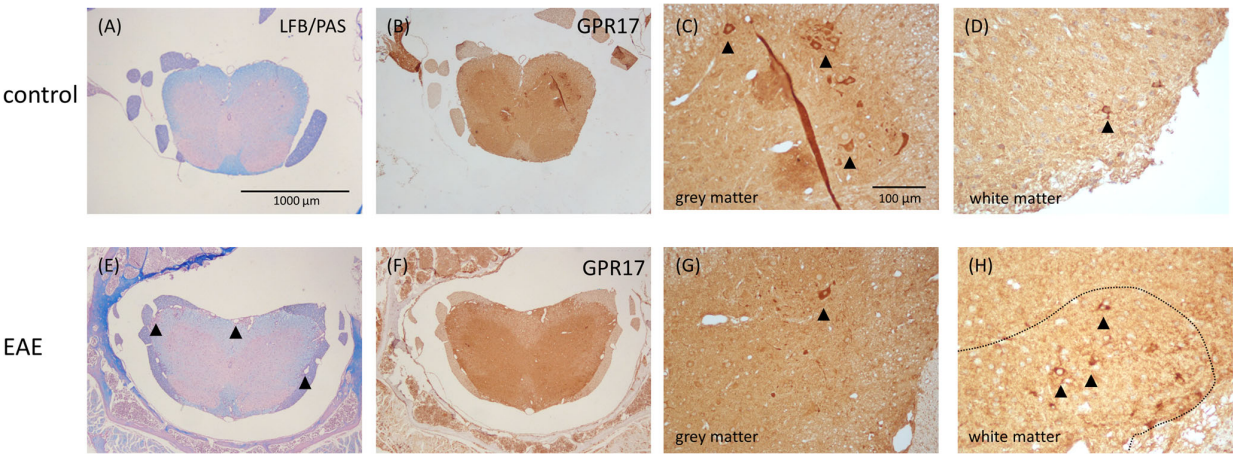

Fig. 8 GPR17 expression in the spinal cord of EAE mice. Representative LFB/PAS stains of spinal cord sections from control (A) and EAE (E) mice. Arrowheads in (E) highlight inflammatory spinal cord white matter lesions. Representative anti-GRP17 stains of spinal cord sections from control (B) and EAE (F) mice. (C, G) show the ventral spinal cord gray matter in higher magnification. Arrowheads highlight GPR17$^+$ motorneurons. (D, H) show the spinal cord white matter in higher magnification. Arrowheads highlight GPR17$^+$ oligodendrocyte progenitor cells. The dotted line in (H) delineates the border of an active inflammatory white matter lesion. Note that densities of GPR17$^+$ cells appear increased in such areas

extent GPR17$^+$ cells differentially contribute to white versus gray matter remyelination is currently unknown. However, our observation of GPR17 induction in the white but not gray matter suggests an important role of GPR17 for delayed cortical remyelination in this model.

MS was long considered a disease of the white matter, but recent magnetic resonance imaging (MRI) and pathology studies have revealed extensive gray matter pathology in MS patients [40]. Since both white and gray mater demyelination significantly contribute to disease burden in MS, it is of vital importance to understand the factors that may hinder or aide successful remyelination in these regions. Obviously, mechanisms operant during white matter remyelination are not necessarily active during gray matter demyelination.

Another interesting outcome of this study is that while GPR17 induction is pronounced at week 5 (i.e., acute demyelination), numbers of GPR17$^+$ cells did not significantly differ from control animals after a 12-week cuprizone intoxication period (i.e., chronic demyelination). Whether this is due to a loss of OPCs in chronic lesions or due to loss of GPR17 expression by OPC remains to be clarified in future studies. However, our finding that lower densities of GPR17$^+$ cells in chronic lesions is paralleled by lower densities of PDGFRα^+ OPCs suggests that OPCs are less abundant in chronic lesions, where remyelination is insufficient.

Of note, GPR17 might not simply be involved in terminal OPC differentiation but potentially regulates oligodendrocyte physiology and pathology in a broader context. Ou and colleagues [13], for example, were able to demonstrate that overexpression or activation of GPR17 in vitro resulted in increased LPC-induced oligodendrocyte apoptosis, whereas GPR17 inhibition reduced oligodendrocyte apoptosis, respectively. At the cellular scale, oligodendrocyte damage can principally spread "centrifugally" (i.e., from the oligodendrocyte cell body to myelin) or "centripetally" (i.e., from myelin to the soma) [41]. In the LPC model and in the inflammatory experimental autoimmune encephalomyelitis model, changes in oligodendrocyte morphology proceed from the myelin sheath to the cell body [41], whereas in the cuprizone model, oligodendrocyte damage spreads centrifugally. It would, thus, be interesting to see whether pharmacological manipulation of GPR17 ameliorates cuprizone-induced apoptosis and whether interference with the GPR17 signaling cascade modulates remyelination in the cuprizone model.

Naturally occurring GPR17 agonists are cysteinyl leukotrienes (CysLTs) such as LTD4 or LTC4 and uracil nucleotides such as UDP, UDP-glucose, and UDP-galactose [16]. It has been suggested that uracil nucleotides can be released from glia cells [42, 43]. Microglia and astrocyte activation are characteristic histopathological hallmarks of MS and its animal models [44–47]. In this context, one might speculate that microglia and astrocyte communicate the presence of brain damage via GPR17 activation to OPCs and by this cell–cell communication network initiate early regenerative processes such as remyelination.

In summary, we were able to demonstrate the expansion of the GPR17$^+$ OPC pool in two different models of toxin-induced demyelination and that this expansion, at least in the cuprizone model, is restricted to the white matter corpus callosum. These data support the interest to evaluate if the pharmacological modulation of the GPR17 signaling cascade could accelerate the remyelination process as already suggested in GPR17 null mice.

Acknowledgements This study was supported by UCB BioPharma (Braine L'Alleud, Belgium), the Dr. Robert Pfleger Stiftung (M.K.), and the Deutsche Forschungsgemeinschaft (KI 1469/8-1). The technical support, H. Helten, P. Ibold, A. Baltruschat, B. Aschauer, JM. Frequin, and M. Caruso, are acknowledged.

Compliance with Ethical Standards

Conflict of interest The authors declare that they have no conflict of interest.

References

1. Aboul-Enein F, Lassmann H (2005) Mitochondrial damage and histotoxic hypoxia: a pathway of tissue injury in inflammatory brain disease? Acta Neuropathol 109(1):49–55. https://doi.org/10.1007/s00401-004-0954-8
2. Smith KJ, Lassmann H (2002) The role of nitric oxide in multiple sclerosis. Lancet Neurol 1(4):232–241
3. Funfschilling U, Supplie LM, Mahad D, Boretius S, Saab AS, Edgar J, Brinkmann BG, Kassmann CM et al (2012) Glycolytic oligodendrocytes maintain myelin and long-term axonal integrity. Nature 485(7399):517–521. https://doi.org/10.1038/nature11007
4. Edgar JM, McLaughlin M, Yool D, Zhang SC, Fowler JH, Montague P, Barrie JA, McCulloch MC et al (2004) Oligodendroglial modulation of fast axonal transport in a mouse model of hereditary spastic paraplegia. J Cell Biol 166(1):121–131. https://doi.org/10.1083/jcb.200312012
5. Uschkureit T, Sporkel O, Stracke J, Bussow H, Stoffel W (2000) Early onset of axonal degeneration in double (plp-/-mag-/-) and hypomyelinosis in triple (plp-/-mbp-/-mag-/-) mutant mice. J Neurosci 20(14):5225–5233
6. Patrikios P, Stadelmann C, Kutzelnigg A, Rauschka H, Schmidbauer M, Laursen H, Sorensen PS, Bruck W et al (2006) Remyelination is extensive in a subset of multiple sclerosis patients. Brain J Neurol 129(Pt 12):3165–3172. https://doi.org/10.1093/brain/awl217
7. Frischer JM, Weigand SD, Guo Y, Kale N, Parisi JE, Pirko I, Mandrekar J, Bramow S et al (2015) Clinical and pathological insights into the dynamic nature of the white matter multiple sclerosis plaque. Ann Neurol 78(5):710–721. https://doi.org/10.1002/ana.24497
8. Xing YL, Roth PT, Stratton JA, Chuang BH, Danne J, Ellis SL, Ng SW, Kilpatrick TJ et al (2014) Adult neural precursor cells from the subventricular zone contribute significantly to oligodendrocyte regeneration and remyelination. J Neurosci 34(42):14128–14146. https://doi.org/10.1523/jneurosci.3491-13.2014
9. Kuhlmann T, Miron V, Cui Q, Wegner C, Antel J, Bruck W (2008) Differentiation block of oligodendroglial progenitor cells as a cause

for remyelination failure in chronic multiple sclerosis. Brain J Neurol 131(Pt 7):1749–1758. https://doi.org/10.1093/brain/awn096
10. Strijbis EMM, Kooi EJ, van der Valk P, Geurts JJG (2017) Cortical remyelination is heterogeneous in multiple sclerosis. J Neuropathol Exp Neurol 76(5):390–401. https://doi.org/10.1093/jnen/nlx023
11. Gudi V, Moharregh-Khiabani D, Skripuletz T, Koutsoudaki PN, Kotsiari A, Skuljec J, Trebst C, Stangel M (2009) Regional differences between grey and white matter in cuprizone induced demyelination. Brain Res 1283:127–138. https://doi.org/10.1016/j.brainres.2009.06.005
12. Baxi EG, DeBruin J, Jin J, Strasburger HJ, Smith MD, Orthmann-Murphy JL, Schott JT, Fairchild AN et al (2017) Lineage tracing reveals dynamic changes in oligodendrocyte precursor cells following cuprizone-induced demyelination. Glia 65(12):2087–2098. https://doi.org/10.1002/glia.23229
13. Ou Z, Sun Y, Lin L, You N, Liu X, Li H, Ma Y, Cao L et al (2016) Olig2-targeted G-protein-coupled receptor Gpr17 regulates oligodendrocyte survival in response to lysolecithin-induced demyelination. J Neurosci 36(41):10560–10573. https://doi.org/10.1523/jneurosci.0898-16.2016
14. Simon K, Hennen S, Merten N, Blattermann S, Gillard M, Kostenis E, Gomeza J (2016) The orphan G protein-coupled receptor GPR17 negatively regulates oligodendrocyte differentiation via Galphai/o and its downstream effector molecules. J Biol Chem 291(2):705–718. https://doi.org/10.1074/jbc.M115.683953
15. Coppi E, Maraula G, Fumagalli M, Failli P, Cellai L, Bonfanti E, Mazzoni L, Coppini R et al (2013) UDP-glucose enhances outward K(+) currents necessary for cell differentiation and stimulates cell migration by activating the GPR17 receptor in oligodendrocyte precursors. Glia 61(7):1155–1171. https://doi.org/10.1002/glia.22506
16. Lecca D, Trincavelli ML, Gelosa P, Sironi L, Ciana P, Fumagalli M, Villa G, Verderio C et al (2008) The recently identified P2Y-like receptor GPR17 is a sensor of brain damage and a new target for brain repair. PLoS One 3(10):e3579. https://doi.org/10.1371/journal.pone.0003579
17. Ciana P, Fumagalli M, Trincavelli ML, Verderio C, Rosa P, Lecca D, Ferrario S, Parravicini C et al (2006) The orphan receptor GPR17 identified as a new dual uracil nucleotides/cysteinyl-leukotrienes receptor. EMBO J 25(19):4615–4627. https://doi.org/10.1038/sj.emboj.7601341
18. Ceruti S, Vigano F, Boda E, Ferrario S, Magni G, Boccazzi M, Rosa P, Buffo A et al (2011) Expression of the new P2Y-like receptor GPR17 during oligodendrocyte precursor cell maturation regulates sensitivity to ATP-induced death. Glia 59(3):363–378. https://doi.org/10.1002/glia.21107
19. Fumagalli M, Daniele S, Lecca D, Lee PR, Parravicini C, Fields RD, Rosa P, Antonucci F et al (2011) Phenotypic changes, signaling pathway, and functional correlates of GPR17-expressing neural precursor cells during oligodendrocyte differentiation. J Biol Chem 286(12):10593–10604. https://doi.org/10.1074/jbc.M110.162867
20. Chen Y, Wu H, Wang S, Koito H, Li J, Ye F, Hoang J, Escobar SS et al (2009) The oligodendrocyte-specific G protein-coupled receptor GPR17 is a cell-intrinsic timer of myelination. Nat Neurosci 12(11):1398–1406. https://doi.org/10.1038/nn.2410
21. Hennen S, Wang H, Peters L, Merten N, Simon K, Spinrath A, Blattermann S, Akkari R et al (2013) Decoding signaling and function of the orphan G protein-coupled receptor GPR17 with a small-molecule agonist. Sci Signal 6(298):ra93. https://doi.org/10.1126/scisignal.2004350
22. Daniele S, Trincavelli ML, Fumagalli M, Zappelli E, Lecca D, Bonfanti E, Campiglia P, Abbracchio MP et al (2014) Does GRK-beta arrestin machinery work as a "switch on" for GPR17-mediated activation of intracellular signaling pathways? Cell Signal 26(6):1310–1325. https://doi.org/10.1016/j.cellsig.2014.02.016
23. Kipp M (2016) Remyelination strategies in multiple sclerosis: a critical reflection. Expert Rev Neurother 16(1):1–3. https://doi.org/10.1586/14737175.2016.1116387
24. Kipp M, Clarner T, Dang J, Copray S, Beyer C (2009) The cuprizone animal model: new insights into an old story. Acta Neuropathol 118(6):723–736. https://doi.org/10.1007/s00401-009-0591-3
25. Huang JK, Jarjour AA, Oumesmar BN, Kerninon C, Williams A, Krezel W, Kagechika H, Bauer J et al (2011) Retinoid X receptor gamma signaling accelerates CNS remyelination. Nat Neurosci 14(1):45–53. https://doi.org/10.1038/nn.2702
26. Slowik A, Schmidt T, Beyer C, Amor S, Clarner T, Kipp M (2015) The sphingosine 1-phosphate receptor agonist FTY720 is neuroprotective after cuprizone-induced CNS demyelination. Br J Pharmacol 172(1):80–92. https://doi.org/10.1111/bph.12938
27. Paxinos G, Franklin KBJ (2001) Mouse brain in stereotaxic coordinates. 2nd ed edn. Academic, San Diego, Calif. ; London,
28. Paxinos G, Watson C The rat brain in stereotaxic coordinates Elsevier Academic Press
29. Ruther BJ, Scheld M, Dreymueller D, Clarner T, Kress E, Brandenburg LO (2017) Combination of cuprizone and experimental autoimmune encephalomyelitis to study inflammatory brain lesion formation and progression. 65 (12):1900–1913. doi:https://doi.org/10.1002/glia.23202
30. Clarner T, Janssen K, Nellessen L, Stangel M, Skripuletz T, Krauspe B, Hess FM, Denecke B et al (2015) CXCL10 triggers early microglial activation in the cuprizone model. J Immunology (Baltimore, Md: 1950) 194(7):3400–3413. https://doi.org/10.4049/jimmunol.1401459
31. Skripuletz T, Lindner M, Kotsiari A, Garde N, Fokuhl J, Linsmeier F, Trebst C, Stangel M (2008) Cortical demyelination is prominent in the murine cuprizone model and is strain-dependent. Am J Pathol 172(4):1053–1061. https://doi.org/10.2353/ajpath.2008.070850
32. Hoflich KM, Beyer C, Clarner T, Schmitz C, Nyamoya S, Kipp M, Hochstrasser T (2016) Acute axonal damage in three different murine models of multiple sclerosis: a comparative approach. Brain Res 1650:125–133. https://doi.org/10.1016/j.brainres.2016.08.048
33. Sahel A, Ortiz FC, Kerninon C, Maldonado PP, Angulo MC, Nait-Oumesmar B (2015) Alteration of synaptic connectivity of oligodendrocyte precursor cells following demyelination. Front Cell Neurosci 9:77. https://doi.org/10.3389/fncel.2015.00077
34. Vigano F, Schneider S, Cimino M, Bonfanti E, Gelosa P, Sironi L, Abbracchio MP, Dimou L (2016) GPR17 expressing NG2-glia: oligodendrocyte progenitors serving as a reserve pool after injury. Glia 64(2):287–299. https://doi.org/10.1002/glia.22929
35. Boda E, Vigano F, Rosa P, Fumagalli M, Labat-Gest V, Tempia F, Abbracchio MP, Dimou L et al (2011) The GPR17 receptor in NG2 expressing cells: focus on in vivo cell maturation and participation in acute trauma and chronic damage. Glia 59(12):1958–1973. https://doi.org/10.1002/glia.21237
36. Boccazzi M, Lecca D, Marangon D, Guagnini F, Abbracchio MP, Ceruti S (2016) A new role for the P2Y-like GPR17 receptor in the modulation of multipotency of oligodendrocyte precursor cells in vitro. Purinergic Signal 12(4):661–672
37. Morrison H, Young K, Qureshi M, Rowe RK, Lifshitz J (2017) Quantitative microglia analyses reveal diverse morphologic responses in the rat cortex after diffuse brain injury. Sci Rep 7(1):13211. https://doi.org/10.1038/s41598-017-13581-z
38. Nimmerjahn A, Kirchhoff F, Helmchen F (2005) Resting microglial cells are highly dynamic surveillants of brain parenchyma in vivo. Science 308(5726):1314–1318. https://doi.org/10.1126/science.1110647
39. Koutsoudaki PN, Hildebrandt H, Gudi V, Skripuletz T, Skuljec J, Stangel M (2010) Remyelination after cuprizone induced demyelination is accelerated in mice deficient in the polysialic acid

synthesizing enzyme St8siaIV. Neuroscience 171(1):235–244. https://doi.org/10.1016/j.neuroscience.2010.08.070
40. Rudick RA, Trapp BD (2009) Gray-matter injury in multiple sclerosis. N Engl J Med 361(15):1505–1506. https://doi.org/10.1056/NEJMcibr0905482
41. Romanelli E, Merkler D, Mezydlo A, Weil MT, Weber MS, Nikic I, Potz S, Meinl E et al (2016) Myelinosome formation represents an early stage of oligodendrocyte damage in multiple sclerosis and its animal model. Nat Commun 7:13275. https://doi.org/10.1038/ncomms13275
42. Lazarowski ER, Shea DA, Boucher RC, Harden TK (2003) Release of cellular UDP-glucose as a potential extracellular signaling molecule. Mol Pharmacol 63(5):1190–1197
43. Kreda SM, Seminario-Vidal L, Heusden C, Lazarowski ER (2008) Thrombin-promoted release of UDP-glucose from human astrocytoma cells. Br J Pharmacol 153(7):1528–1537. https://doi.org/10.1038/sj.bjp.0707692
44. Skripuletz T, Hackstette D, Bauer K, Gudi V, Pul R, Voss E, Berger K, Kipp M et al (2013) Astrocytes regulate myelin clearance through recruitment of microglia during cuprizone-induced demyelination. Brain J Neurol 136(Pt 1):147–167. https://doi.org/10.1093/brain/aws262
45. Grosse-Veldmann R, Becker B, Amor S, van der Valk P, Beyer C, Kipp M (2016) Lesion expansion in experimental demyelination animal models and multiple sclerosis lesions. Mol Neurobiol 53(7):4905–4917. https://doi.org/10.1007/s12035-015-9420-y
46. van Horssen J, Singh S, van der Pol S, Kipp M, Lim JL, Peferoen L, Gerritsen W, Kooi EJ et al (2012) Clusters of activated microglia in normal-appearing white matter show signs of innate immune activation. J Neuroinflammation 9:156. https://doi.org/10.1186/1742-2094-9-156
47. Lassmann H, van Horssen J, Mahad D (2012) Progressive multiple sclerosis: pathology and pathogenesis. Nat Rev Neurol 8(11):647–656. https://doi.org/10.1038/nrneurol.2012.168

7. Veröffentlichung II

Leopold P, Schmitz C, Kipp M:

Animal Weight Is an Important Variable for Reliable Cuprizone-Induced Demyelination.

Journal of molecular neuroscience, 2019, Springer Nature

Journal of Molecular Neuroscience (2019) 68:522–528
https://doi.org/10.1007/s12031-019-01312-0

Animal Weight Is an Important Variable for Reliable Cuprizone-Induced Demyelination

Patrizia Leopold[1,2] · Christoph Schmitz[2] · Markus Kipp[1]

Received: 11 January 2019 / Accepted: 22 March 2019 / Published online: 2 April 2019

Abstract
An elegant model to study mechanisms operant during oligodendrocyte degeneration and subsequent demyelination is the cuprizone model. In that model, mice are intoxicated with the copper chelation agent cuprizone which results in early oligodendrocyte stress, oligodendrocyte apoptosis, and, finally, demyelination. Here, we systematically investigated to what extent the animals' weight at the beginning of the cuprizone intoxication period is critical for the reproducibility of the cuprizone-induced pathology. We can demonstrate that a negative correlation exists between the two variables "extent of cuprizone-induced demyelination" and "starting weight." Demyelination and microglia activation were more severe in low weight compared to heavy weight mice. These findings are highly relevant for the experimental design using the cuprizone model.

Keywords Cuprizone · Oligodendrocyte degeneration · Weight · Correlation

Introduction

Multiple sclerosis (MS), a neurodegenerative and inflammatory disorder of the central nervous system (CNS), is associated with the development of demyelinated plaques, oligodendrocyte destruction, and axonal degeneration. These pathological processes are paralleled by the activation of astrocytes and microglia, as well as the recruitment of peripheral immune cells into the CNS (van der Valk and De Groot 2000).

Oligodendrocytes are the myelin-forming cells in the CNS, are essential for the propagation of action potentials along axons, and additionally serve to support neurons by, for example, providing nutritional support (Funfschilling et al. 2012). Initially, MS lesions were thought to result from focal inflammation causing a rapid loss of oligodendrocytes and myelin. In contrast to that view, several authors noted the presence of oligodendrocytes in early MS lesions (Lassmann 1983; Raine et al. 1981). To date, several underlying mechanisms leading to oligodendrocyte degeneration in MS are discussed, among pore-forming proteins released by lymphocytes such as perforin (Scolding et al. 1990), antibodies (Genain et al. 1999), oxidative injury/stress (Fischbach et al. 2018; Lassmann and van Horssen 2016; Licht-Mayer et al. 2015), or mitochondrial dysfunction (Mahad et al. 2008). Of note, there is no oligodendrocyte-based treatment of MS and all the available disease-modifying agents target exclusively immune mechanisms, providing little direct protection to oligodendrocytes and their myelin sheaths (Behrangi et al. 2019). A better understanding of oligodendrocyte degeneration in MS is, therefore, urgently needed.

One elegant model to study mechanisms operant during oligodendrocyte degeneration and subsequent demyelination is the cuprizone model (Kipp et al. 2017; Zendedel et al. 2013). In that model, mice are intoxicated with the copper chelation agent cuprizone which results in early oligodendrocyte stress (Goldberg et al. 2013), oligodendrocyte apoptosis (Hesse et al. 2010), and, finally, demyelination (Schmidt et al. 2013). A number of signaling cascades have been described to regulate demyelination in this model including chemokines (Clarner et al. 2015), steroid hormones (Acs et al. 2009), stress-associated transcription factors (Fischbach et al. 2018), and energy metabolism regulators (Xing et al. 2018). In most studies, the cuprizone intoxication is realized by per os administration by mixing the pulverized cuprizone either with ground rodent chow or by oral gavage of solubilized cuprizone. While sex and genetic background of the animals have been identified as important variables for the reproducibility and the extent of cuprizone-induced pathological

✉ Markus Kipp
Markus.kipp@med.uni-rostock.de

[1] Institute of Anatomy, Rostock University Medical Center, 18057 Rostock, Germany

[2] Department of Anatomy II, Ludwig-Maximilians-University of Munich, 80336 Munich, Germany

changes, the variable "weight" as a critical variable for reliable and consistent demyelination has so far not been systematically addressed. However, it is likely that systemic concentrations of the cuprizone toxin are higher in low weight compared to heavy weight mice, and that pronounced differences in the variable "weight" might impact on experimental outcomes.

In this study, we therefore systematically investigated the correlation of the variable "weight at the first day of cuprizone intoxication" with the variables "oligodendrocyte apoptosis," "microglia activation," and "demyelination."

Materials and Methods

Animals, Experimental Groups, and Tissue Sampling

Six- to 10-week-old C57BL/6 mice (17–27 g) were used from the animal facility of the LMU Munich University (Max von Pettenkofer Institute). Microbiological monitoring was performed according to the Federation of European Laboratory Animal Science Associations recommendations. A maximum of five animals were housed per cage (cage area 435 cm^2). Animals were kept under standard laboratory conditions (12-h light/12-h dark cycle, controlled temperature 22 °C ± 2 °C, and 50% ± 10% humidity) with access to food and water ad libitum. It was assured that researchers and technicians did not use any light during the night cycle period. All experiments were formally approved by the *Regierung Oberbayern* (reference number 55.2-154-2532-73-15). Cuprizone intoxication was performed for 1 ($n = 9$) or three ($n = 7$ for females; $n = 5$ for males) weeks as described previously in detail (Chrzanowski et al. 2019; Hochstrasser et al. 2017). Control animals received a diet of standard rodent chow for the entire duration of the study. For histological and immunohistochemical studies, mice were anesthetized with ketamine (100 mg kg^{-1} i.p.) and xylazine (10 mg kg^{-1} i.p.), and then transcardially perfused with ice-cold PBS followed by a 3.7% formaldehyde solution (pH 7.4). Brains were postfixed overnight in a 3.7% formaldehyde solution at 4 °C, dissected, and embedded in paraffin, and then coronal sections (5 μm) were prepared (Acs et al. 2009; Clarner et al. 2012).

Immunohistochemistry/Histochemistry and Evaluation

For immunohistochemistry, sections were rehydrated and, if necessary, antigens were unmasked by heating in Tris/EDTA (pH 9.0) or citrate (pH 6.0) buffer. After washing in PBS, sections were blocked in blocking solution (serum of the species in which the secondary antibody was produced) for 1 h. Then, the sections were incubated overnight (4 °C) with primary antibodies diluted in blocking solution. Primary and secondary antibodies used in this study are listed in Table 1. The next day, slides were incubated in 0.3% hydrogen peroxide/PBS for 30 min and then incubated with biotinylated secondary antibodies for 1 h followed by peroxidase-coupled avidin-biotin complex (ABC kit; Vector Laboratories, Peterborough, UK). Sections were finally exposed to 3,3′-diaminobenzidine (DAKO, Santa Clara, CA, USA) as a peroxidase substrate. To visualize cell nuclei, sections were stained with hematoxylin solution. Negative control sections without primary antibodies were processed to ensure specificity of the staining. Luxol fast blue (LFB)/periodic acid-Schiff (PAS) stains were performed following standard protocols (Nack et al. 2019; Nyamoya et al. 2018). The stained and processed sections were digitalized using a Nikon ECLIPSE 50i microscope (Nikon, Nikon Instruments, Düsseldorf, Germany) equipped with a DS-2Mv camera. The open-source program ImageJ 1.48v (NIH, Bethesda, MD, USA) was used to determine cellular densities (cells/mm^2) and to evaluate staining intensity using semi-automated densitometrical evaluation after threshold setting. In brief, acquired images were converted to gray scale images, and a global thresholding algorithm was used for dividing each image into two classes of pixels (black and white, i.e., binary conversion). Global thresholding works by choosing a value cutoff, such that every pixel less than that value is considered one class, while every pixel greater than that value is considered the other class. Relative staining intensity was then quantified in binary converted images, and the results are presented as percentage area.

Statistical Analyses

Statistical analyses were performed using Prism 5 (GraphPad Software Inc., San Diego, CA, USA). All data are given as arithmetic means ± SEMs. Correlation analyses between the variable "weight" and histological parameters were performed by calculating Pearson's correlation coefficient r, R^2, and a two-tailed p value. A p value of < 0.05 was considered to be statistically significant. No outliers were excluded from the analyses. The Shapiro-Wilk test was applied to test for normal data distribution.

Results

First, we were interested whether the weight of the animals before the initiation of the cuprizone intoxication is an important factor for the severity of early oligodendrocyte apoptosis and concomitant microglia activation. Therefore, in a first step, animals were intoxicated with cuprizone for 1 week, and the densities of apoptotic oligodendrocytes (H&E) and microglia cells (anti-IBA1) were analyzed in the corpus callosum at the level of the rostral hippocampus (see Fig. 1a). After 1 week of cuprizone intoxication, all mice lost

Table 1 Primary antibodies and secondary antibodies used

Antigen Primary antibodies	Host	Dilution	Antigen retrieval	Purchase number	RRID	Manufacturer
PLP	Mouse	1:5000	None	MCA839G	AB_2237198	Bio-Rad Laboratories Inc., Germany
IBA1	Rabbit	1:5000	Tris/EDTA	019-19741	AB_839504	Wako, USA
OLIG2	Rabbit	1:2000	Tris/EDTA	Ab9610	AB_570666	Merck-Millipore, Germany
Biotinylated secondary antibodies						
Goat anti-rabbit IgG	Goat	1:200	Not applicable	BA-1000	AB_2313606	Vector Laboratories, Burlingame, USA
Goat anti-mouse IgG	Goat	1:200	Not applicable	BA-9200	AB_2336171	Vector Laboratories, Burlingame, USA

weight ranging from 19.9 to 1.5% (data not shown). Neither the densities of apoptotic bodies (Pearson's correlation coefficient $r = -0.08466$; $R^2 = 0.007167$; two-tailed p value = 0.8286) nor the densities of IBA1$^+$ microglia cells (Pearson's correlation coefficient $r = -0.2022$; $R^2 = 0.04090$; two-tailed p value = 0.6018) correlated to the weight of the animals (see Fig. 1b, c). Furthermore, we did not find any correlation between the densities of OLIG2-expressing oligodendrocytes (Pearson's correlation coefficient $r = -0.04941$; $R^2 = 0.002441$; two-tailed p value = 0.8996) and the starting weight of the animals (see Fig. 1d). These results suggest that irrespective of the animal weight, cuprizone intoxication results in profound oligodendrocyte apoptosis with concomitant microglia activation.

Next, we focused on week 3 at the time at which first signs of demyelination can be observed on the histopathological level. After week 3, all mice showed a reduced weight compared to their starting weight ranging from 12.1 to 1.0%. Anti-PLP staining intensity positively correlated with the weight of the animals (Pearson's correlation coefficient $r = 0.5661$; $R^2 = 0.3205$; two-tailed p value = 0.0348). As higher the starting weight at the beginning of the cuprizone intoxication period, as less severe loss of anti-PLP staining intensity was observed (see Fig. 2a). A similar yet non-significant trend was observed for LFB/PAS-stained sections (Pearson's correlation coefficient $r = 0.5516$; $R^2 = 0.3042$; two-tailed p value = 0.1993) (see Fig. 2b). To further substantiate our observation that the cuprizone-induced pathology is more severe in animals with a low starting weight, we assessed microgliosis by either counting the densities of IBA1$^+$ cells, or by measuring the optical density in anti-IBA1-stained sections. As demonstrated in Fig. 2c, d, we found a significant negative correlation between the densities of IBA1$^+$ cells per square millimeter and the starting weight (Pearson's correlation coefficient $r = -0.8660$; $R^2 = 0.7500$; two-tailed p value = 0.0117). A similar yet non-significant trend was observed if microglia activation was assessed by optical densitometry measurements (Pearson's correlation coefficient $r = -0.6196$; $R^2 = 0.3839$; two-tailed p value = 0.1378). Finally, we repeated these experiments with male mice to study a potential gender bias in our results. LFB staining intensity strongly correlated with the weight of the animals in male mice (Pearson's correlation coefficient $r = 0.9669$; $R^2 = 0.9349$; two-tailed p value = 0.072). Furthermore, a similar, yet not significant and moderate correlation was observed between IBA1$^+$ cell densities and the animals' weight (Pearson's correlation coefficient $r = -0.5201$; $R^2 = 0.2705$; two-tailed p value = 0.1512) (see Fig. 2e).

Discussion

The neurotoxin cuprizone is increasingly used to study cell-cell interactions and molecular pathways mediating CNS demyelination and remyelination. Such studies are usually performed to understand disease-relevant pathologies operant in MS patients or, more recently, to understand schizophrenia-relevant abnormalities (Valeiras et al. 2014). The value of this model for such studies on the one hand depends on an accurate description of its quantifiable features, on the other hand on reliable protocols to induce consistent and reproducible demyelination. A number of variables have been identified in the past to be important for such a reproducible demyelination, among gender (Taylor et al. 2009; Valeiras et al. 2014), sex chromosomes (Moore et al. 2013), genetic background (Taylor et al. 2009), or the level of circulating sex hormones (Patel et al. 2013). Surprisingly, the variable weight was never systematically analyzed as an important factor for reliable cuprizone-induced demyelination.

This study clearly demonstrates that animal weight is an important variable for reliable cuprizone-induced demyelination at week 3. It is currently not clear why we did observe a correlation between the cuprizone-induced pathology and the starting weight at week 3, but not at week 1. As demonstrated in Fig. 1, the densities of apoptotic oligodendrocytes (quantified in H&E-stained sections), the extent of early microglia activation, or the densities of (surviving) oligodendrocytes (quantified in anti-OLIG2-stained sections) did not correlate with the starting weight of the animals. We have recently shown that

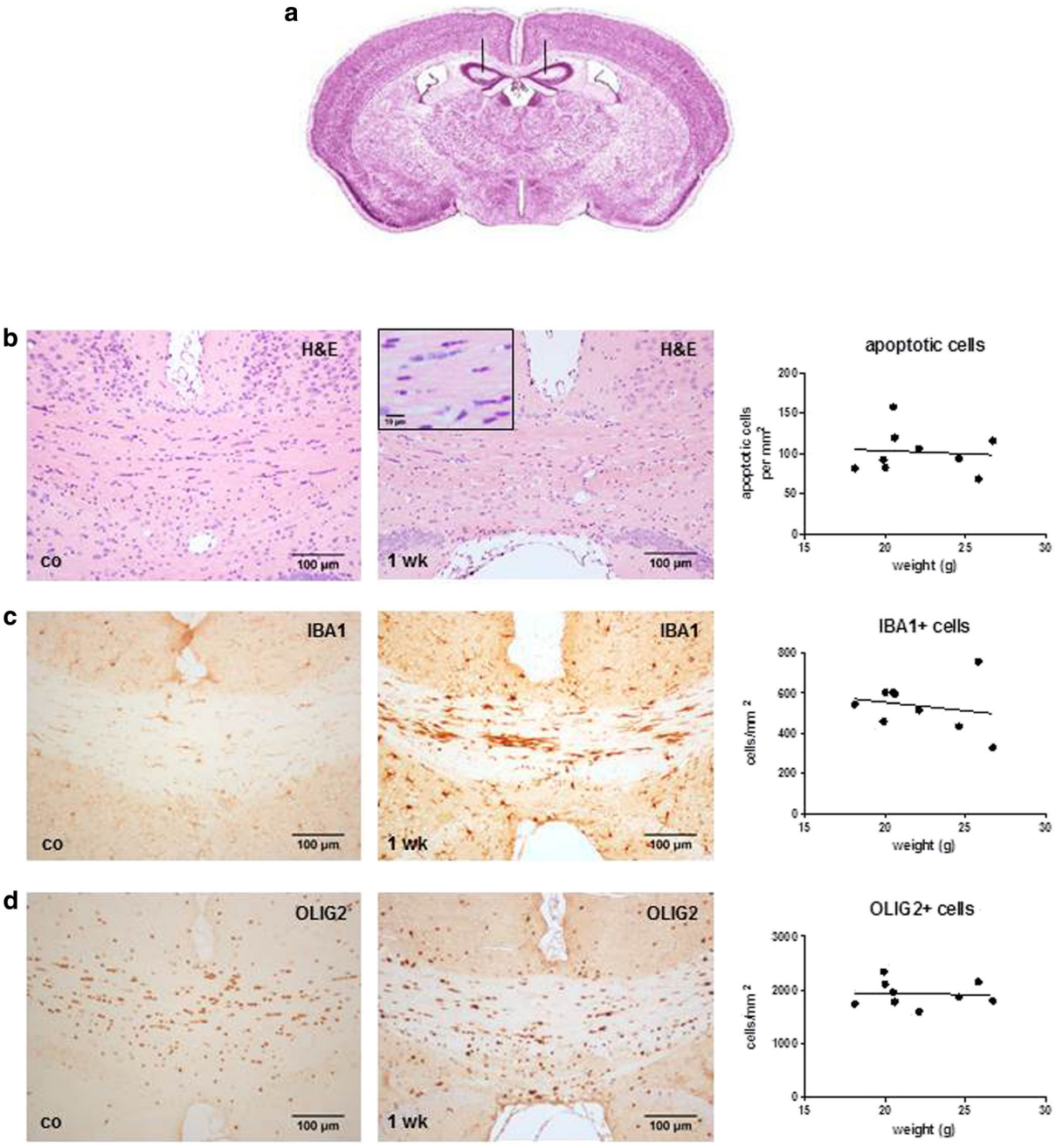

Fig. 1 Animals of different weight are equally vulnerable to cuprizone-induced oligodendrocyte apoptosis at week 1. **a** Schematic illustrating the brain level analyzed during the study. The two black lines outline the lateral borders of the mCC (medial corpus callosum). **b** Representative H&E stain illustrating apoptotic cells in control mice and after 1-week cuprizone intoxication is shown at the left, and a scatterplot of the two variables "weight" and "apoptotic cells per mm^2" is shown at the right. The best fit regression line is included. **c** Representative anti-IBA1 stains illustrating microglia densities in control mice and after 1-week cuprizone intoxication. A scatterplot of the two variables "weight" and "$IBA1^+$ cells per mm^2" is shown at the right. The best fit regression line is included. **d** Representative anti-OLIG2 stains illustrating oligodendrocyte densities in control mice and after 1-week cuprizone intoxication. A scatterplot of the two variables "weight" and "$OLIG2^+$ cells per mm^2" is shown at the right. The best fit regression line is included

oligodendrocytes react with differing sensitivity to the toxic insult, with some cells dying early during lesion development and some cells being resistant for weeks (Fischbach et al. 2018). We assume that the highly vulnerable oligodendrocyte population,

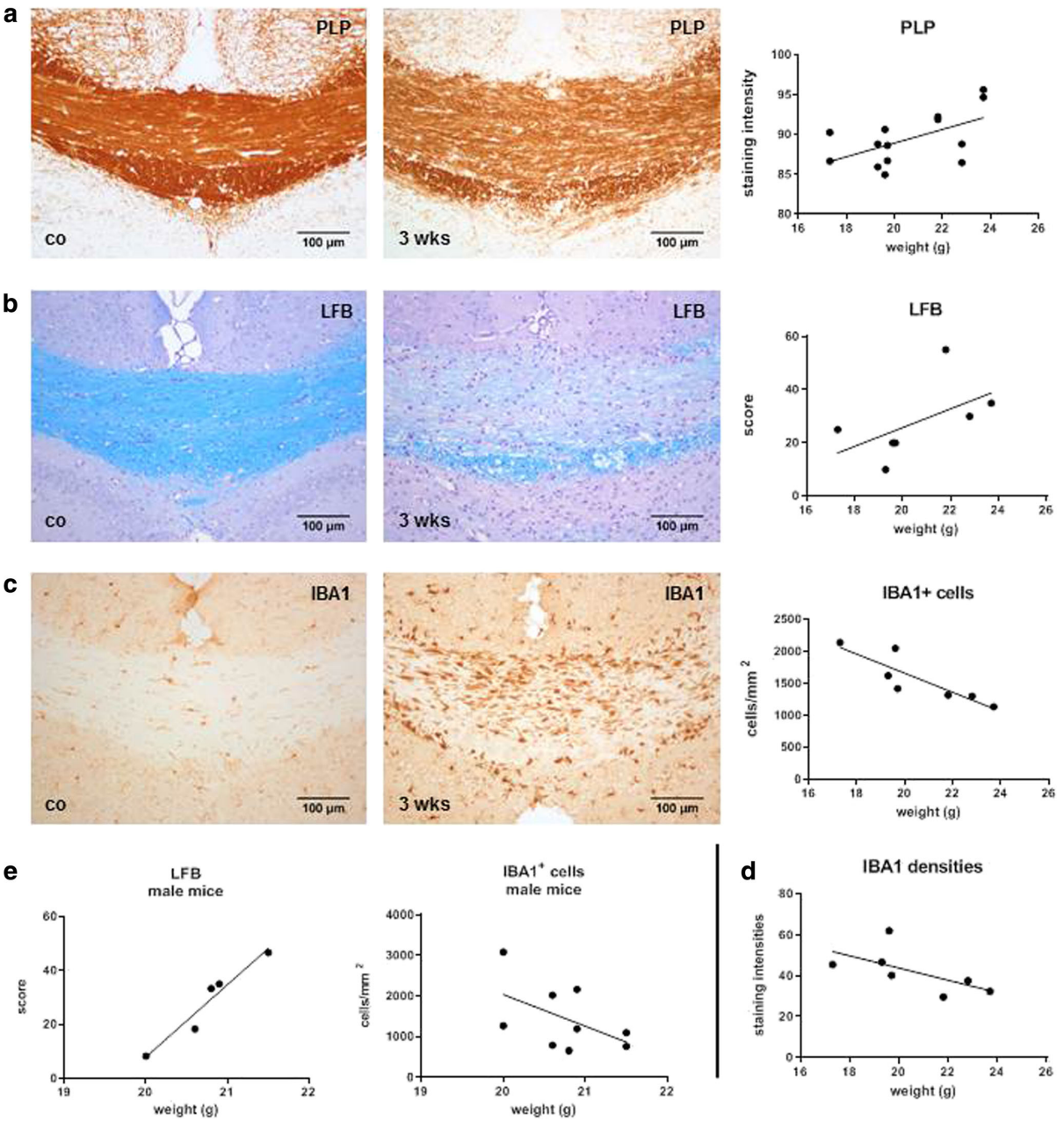

Fig. 2 Animals with higher weight are less vulnerable to cuprizone-induced pathology at week 3. **a** Representative anti-PLP stain illustrating myelination in control mice and after 3-week cuprizone intoxication is shown at the left, a scatterplot of the two variables "weight" and "myelination" is shown at the right. The best fit regression line is included. **b** Representative LFB/PAS stains illustrating myelination in control mice and after 3-week cuprizone intoxication is shown at the left, and a scatterplot of the two variables "weight" and "myelination" is shown at the right. The best fit regression line is included. **c** Representative anti-IBA1 stains illustrating microglia densities in control mice and after 3-week cuprizone intoxication. A scatterplot of the two variables "weight" and "IBA1$^+$ cells per mm^2" is shown at the right. The best fit regression line is included. **d** Scatterplot of the two variables "weight" and "IBA1$^+$ staining intensity." The best fit regression line is included. Note that female mice were used for the results shown in **a**–**d**. **e** Scatterplot of the two variables "weight" and "myelination" is shown at the left, and scatterplot of the two variables "weight" and "IBA1$^+$ cells per mm^2" is shown at the right. The best fit regression line is included. Note that male mice were used for these results

which is subjected to apoptosis during the first week, is vulnerable even if cuprizone concentrations within the brain are low. In such a *scenario*, we might miss any correlation between weight and oligodendrocyte vulnerability at week 1 because of too high cuprizone intoxication levels. The situation might be different at week 3. Those oligodendrocytes which are more resistant against the systemic cuprizone intoxication protocol probably require higher cuprizone concentrations to be subjected to apoptosis. In such a *scenario*, a correlation can be detected. Alternatively, it might be that the activation of microglia cells, which phagocytose myelin during the course of the cuprizone intoxication period, is not merely activated by the dying oligodendrocytes but additionally by high systemic cuprizone concentrations as suggested by Pasquini and colleagues (Pasquini et al. 2007). However, whether this is true or not requires further studies.

This is, to the best of our knowledge, the first study demonstrating that a negative correlation exists between the two variables "extent of cuprizone-induced demyelination" and "starting weight" (i.e., the weight of the animal at the beginning of the cuprizone intoxication). Given the fact that much higher concentrations of cuprizone have to be used to induce demyelination in rats compared to mice (Love 1988; Omotoso et al. 2018), such a finding is maybe not surprising, but highly relevant for the experimental design of future studies. In our hands, we obtain best results if we order male mice at an age of 6–7 weeks with a weight ranging from 18 to 20 g. Of note, the weight of the animals should be determined after 1 week of rest because, due to the transport-induced stress, the mice show considerable weight loss.

The results shown in this study are obtained from wild-type mice used to analyze the relevance of an endoplasmic reticulum stress cascade for cuprizone-induced demyelination (Fischbach et al. 2018). Especially in animal facilities with place limitations, it is in many cases not possible to design the experiment in a way that all mice have a similar weight at the beginning of a cuprizone intoxication period. In such a case, one should try to balance the weight between the different study groups in a way that light weight and heavy weight mice are equally distributed among the groups. Of note, a negative correlation between starting weight and the extent of demyelination at week 3 has as well been observed in the knockout mice, showing that such an effect is not restricted to wild-type animals.

Acknowledgements The technical support from S. Wübbel, B. Aschauer, and A. Baltruschat is acknowledged.

Funding Information This study was financially supported by the Deutsche Forschungsgemeinschaft (KI 1469/8-1).

Compliance with Ethical Standards

All experiments were formally approved by the *Regierung Oberbayern* (reference number 55.2-154-2532-73-15).

Conflict of Interest The authors declare that they have no competing interests.

References

Acs P, Kipp M, Norkute A, Johann S, Clarner T, Braun A, Berente Z, Komoly S, Beyer C (2009) 17beta-estradiol and progesterone prevent cuprizone provoked demyelination of corpus callosum in male mice. Glia 57:807–814. https://doi.org/10.1002/glia.20806

Behrangi N, Fischbach F, Kipp M (2019) Mechanism of siponimod: anti-inflammatory and neuroprotective mode of action Cells 8 doi:https://doi.org/10.3390/cells8010024

Chrzanowski U, Schmitz C, Horn-Bochtler A, Nack A, Kipp M (2019) Evaluation strategy to determine reliable demyelination in the cuprizone model. Metab Brain Dis 34:681–685. https://doi.org/10.1007/s11011-018-0375-3

Clarner T, Diederichs F, Berger K, Denecke B, Gan L, van der Valk P, Beyer C, Amor S, Kipp M (2012) Myelin debris regulates inflammatory responses in an experimental demyelination animal model and multiple sclerosis lesions. Glia 60:1468–1480. https://doi.org/10.1002/glia.22367

Clarner T, Janssen K, Nellessen L, Stangel M, Skripuletz T, Krauspe B, Hess FM, Denecke B, Beutner C, Linnartz-Gerlach B, Neumann H, Vallières L, Amor S, Ohl K, Tenbrock K, Beyer C, Kipp M (2015) CXCL10 triggers early microglial activation in the cuprizone model. Journal of immunology (Baltimore, Md : 1950) 194:3400–3413. https://doi.org/10.4049/jimmunol.1401459

Fischbach F, Nedelcu J, Leopold P, Zhan J, Clarner T, Nellessen L, Beißel C, van Heuvel Y, Goswami A, Weis J, Denecke B, Schmitz C, Hochstrasser T, Nyamoya S, Victor M, Beyer C, Kipp M (2018) Cuprizone-induced graded oligodendrocyte vulnerability is regulated by the transcription factor DNA damage-inducible transcript 3. Glia 67:263–276. https://doi.org/10.1002/glia.23538

Funfschilling U et al (2012) Glycolytic oligodendrocytes maintain myelin and long-term axonal integrity. Nature 485:517–521. https://doi.org/10.1038/nature11007

Genain CP, Cannella B, Hauser SL, Raine CS (1999) Identification of autoantibodies associated with myelin damage in multiple sclerosis. Nat Med 5:170–175. https://doi.org/10.1038/5532

Goldberg J, Daniel M, van Heuvel Y, Victor M, Beyer C, Clarner T, Kipp M (2013) Short-term cuprizone feeding induces selective amino acid deprivation with concomitant activation of an integrated stress response in oligodendrocytes. Cell Mol Neurobiol 33:1087–1098. https://doi.org/10.1007/s10571-013-9975-y

Hesse A, Wagner M, Held J, Brück W, Salinas-Riester G, Hao Z, Waisman A, Kuhlmann T (2010) In toxic demyelination oligodendroglial cell death occurs early and is FAS independent. Neurobiol Dis 37:362–369. https://doi.org/10.1016/j.nbd.2009.10.016

Hochstrasser T, Exner GL, Nyamoya S, Schmitz C, Kipp M (2017) Cuprizone-containing pellets are less potent to induce consistent demyelination in the corpus callosum of C57BL/6 mice. J Mol Neurosci 61:617–624. https://doi.org/10.1007/s12031-017-0903-3

Kipp M, Nyamoya S, Hochstrasser T, Amor S (2017) Multiple sclerosis animal models: a clinical and histopathological perspective. Brain pathology (Zurich, Switzerland) 27:123–137. https://doi.org/10.1111/bpa.12454

Lassmann H (1983) Comparative neuropathology of chronic experimental allergic encephalomyelitis and multiple sclerosis. Schriftenreihe Neurologie 25:1–135

Lassmann H, van Horssen J (2016) Oxidative stress and its impact on neurons and glia in multiple sclerosis lesions. Biochim Biophys Acta 1862:506–510. https://doi.org/10.1016/j.bbadis.2015.09.018

Licht-Mayer S, Wimmer I, Traffehn S, Metz I, Brück W, Bauer J, Bradl M, Lassmann H (2015) Cell type-specific Nrf2 expression in

multiple sclerosis lesions. Acta Neuropathol 130:263–277. https://doi.org/10.1007/s00401-015-1452-x
Love S (1988) Cuprizone neurotoxicity in the rat: morphologic observations. J Neurol Sci 84:223–237
Mahad D, Ziabreva I, Lassmann H, Turnbull D (2008) Mitochondrial defects in acute multiple sclerosis lesions. Brain : a journal of neurology 131:1722–1735. https://doi.org/10.1093/brain/awn105
Moore S, Patel R, Hannsun G, Yang J, Tiwari-Woodruff SK (2013) Sex chromosome complement influences functional callosal myelination. Neuroscience 245:166–178. https://doi.org/10.1016/j.neuroscience.2013.04.017
Nack A, Brendel M, Nedelcu J, Daerr M, Nyamoya S, Beyer C, Focke C, Deussing M, Hoornaert C, Ponsaerts P, Schmitz C, Bartenstein P, Rominger A, Kipp M (2019) Expression of translocator protein and [18F]-GE180 ligand uptake in multiple sclerosis animal models. Cells 8. https://doi.org/10.3390/cells8020094
Nyamoya S, Leopold P, Becker B, Beyer C, Hustadt F, Schmitz C, Michel A, Kipp M (2018) G-protein-coupled receptor Gpr17 expression in two multiple sclerosis remyelination models. Mol Neurobiol 56:1109–1123. https://doi.org/10.1007/s12035-018-1146-1
Omotoso GO, Gbadamosi IT, Afolabi TT, Abdulwahab AB, Akinlolu AA (2018) Ameliorative effects of Moringa on cuprizone-induced memory decline in rat model of multiple sclerosis. Anatomy & cell biology 51:119–127. https://doi.org/10.5115/acb.2018.51.2.119
Pasquini LA, Calatayud CA, Bertone Una AL, Millet V, Pasquini JM, Soto EF (2007) The neurotoxic effect of cuprizone on oligodendrocytes depends on the presence of pro-inflammatory cytokines secreted by microglia. Neurochem Res 32:279–292. https://doi.org/10.1007/s11064-006-9165-0
Patel R, Moore S, Crawford DK, Hannsun G, Sasidhar MV, Tan K, Molaie D, Tiwari-Woodruff SK (2013) Attenuation of corpus callosum axon myelination and remyelination in the absence of circulating sex hormones. Brain pathology (Zurich, Switzerland) 23:462–475. https://doi.org/10.1111/bpa.12029
Raine CS, Scheinberg L, Waltz JM (1981) Multiple sclerosis. Oligodendrocyte survival and proliferation in an active established lesion. Laboratory investigation; a journal of technical methods and pathology 45:534–546
Schmidt T, Awad H, Slowik A, Beyer C, Kipp M, Clarner T (2013) Regional heterogeneity of cuprizone-induced demyelination: topographical aspects of the midline of the corpus callosum. J Mol Neurosci 49:80–88. https://doi.org/10.1007/s12031-012-9896-0
Scolding NJ, Jones J, Compston DA, Morgan BP (1990) Oligodendrocyte susceptibility to injury by T-cell perforin. Immunology 70:6–10
Taylor LC, Gilmore W, Matsushima GK (2009) SJL mice exposed to cuprizone intoxication reveal strain and gender pattern differences in demyelination. Brain pathology (Zurich, Switzerland) 19:467–479. https://doi.org/10.1111/j.1750-3639.2008.00230.x
Valeiras B, Rosato Siri MV, Codagnone M, Reines A, Pasquini JM (2014) Gender influence on schizophrenia-relevant abnormalities in a cuprizone demyelination model. Glia 62:1629–1644. https://doi.org/10.1002/glia.22704
van der Valk P, De Groot CJ (2000) Staging of multiple sclerosis (MS) lesions: pathology of the time frame of MS. Neuropathol Appl Neurobiol 26:2–10
Xing B, Brink LE, Maers K, Sullivan ML, Bodnar RJ, Stolz DB, Cambi F (2018) Conditional depletion of GSK3b protects oligodendrocytes from apoptosis and lessens demyelination in the acute cuprizone model. Glia 66:1999–2012. https://doi.org/10.1002/glia.23453
Zendedel A, Beyer C, Kipp M (2013) Cuprizone-induced demyelination as a tool to study remyelination and axonal protection. J Mol Neurosci 51:567–572. https://doi.org/10.1007/s12031-013-0026-4

8. Literaturverzeichnis

1. Kipp, M., et al., *Multiple sclerosis animal models: a clinical and histopathological perspective.* Brain Pathol, 2017. **27**(2): p. 123-137.
2. WorldHealthOrganisation, *Atlas multiple sclerosis resources in the world 2008*. 2008, Geneva: WHO Press. 56.
3. Rhead, B., et al., *Mendelian randomization shows a causal effect of low vitamin D on multiple sclerosis risk.* Neurol Genet, 2016. **2**(5): p. e97.
4. Ascherio, A. and K.L. Munger, *Epidemiology of Multiple Sclerosis: From Risk Factors to Prevention-An Update.* Semin Neurol, 2016. **36**(2): p. 103-14.
5. Bender, A., et al., *Kurzlehrbuch Neurologie, 3. Auflage*. 2018: Elsevier.
6. Thompson, A.J., et al., *Diagnosis of multiple sclerosis: 2017 revisions of the McDonald criteria.* The Lancet. Neurology, 2018. **17**(2): p. 162-173.
7. Lublin, F.D., et al., *Defining the clinical course of multiple sclerosis: the 2013 revisions.* Neurology, 2014. **83**(3): p. 278-286.
8. Brownlee, W.J., et al., *Diagnosis of multiple sclerosis: progress and challenges.* Lancet (London, England), 2017. **389**(10076): p. 1336-1346.
9. Fisniku, L.K., et al., *Disability and T2 MRI lesions: a 20-year follow-up of patients with relapse onset of multiple sclerosis.* Brain : a journal of neurology, 2008. **131**(Pt 3): p. 808-817.
10. Miller, D.H. and S.M. Leary, *Primary-progressive multiple sclerosis.* The Lancet. Neurology, 2007. **6**(10): p. 903-912.
11. Mahad, D.H., B.D. Trapp, and H. Lassmann, *Pathological mechanisms in progressive multiple sclerosis.* The Lancet. Neurology, 2015. **14**(2): p. 183-193.
12. Stys, P.K., et al., *Will the real multiple sclerosis please stand up?* Nature reviews. Neuroscience, 2012. **13**(7): p. 507-514.
13. Owen, T., *Multiple sclerosis.* Can J Occup Ther, 1957. **24**(4): p. 125-9.
14. Kurtzke, J.F., *Rating neurologic impairment in multiple sclerosis: an expanded disability status scale (EDSS).* Neurology, 1983. **33**(11): p. 1444-1452.
15. Filippi, M., et al., *Assessment of lesions on magnetic resonance imaging in multiple sclerosis: practical guidelines.* Brain : a journal of neurology, 2019. **142**(7): p. 1858-1875.
16. McDonald, W.I., et al., *Recommended diagnostic criteria for multiple sclerosis: guidelines from the International Panel on the diagnosis of multiple sclerosis.* Ann Neurol, 2001. **50**(1): p. 121-7.
17. Thompson, E.J., et al., *Oligoclonal immunoglobulins and plasma cells in spinal fluid of patients with multiple sclerosis.* British medical journal, 1979. **1**(6155): p. 16-17.
18. Tintoré, M., et al., *Do oligoclonal bands add information to MRI in first attacks of multiple sclerosis?* Neurology, 2008. **70**(13 Pt 2): p. 1079-1083.
19. Halliday, A.M., W.I. McDonald, and J. Mushin, *Visual evoked response in diagnosis of multiple sclerosis.* British medical journal, 1973. **4**(5893): p. 661-664.
20. Gold, R., *DIagnose und THerapie der Multiplen Sclerose: S2-Leitlinie.* Deutsche Gesellschaft für Neurologie, 2012.
21. Hoché, G. and L.J. Sanders, *On some arthropathies apparently related to a lesion of the brain or spinal cord, by Dr. J.-M. Charcot, January 1868.* J Hist Neurosci, 1992. **1**(1): p. 75-87.
22. Charcot, M., *Histologie de la sclerose en plaque.* Gaz Hop (Paris), 1868: p. 554-556.

23. Silverthorn, D., *Physiologie, 4. Auflage*. 2009: Pearson Studium
24. Lee, Y., et al., *Oligodendroglia metabolically support axons and contribute to neurodegeneration.* Nature, 2012. **487**(7408): p. 443-8.
25. Rowitch, D.H. and A.R. Kriegstein, *Developmental genetics of vertebrate glial-cell specification.* Nature, 2010. **468**(7321): p. 214-22.
26. Zhang, H. and R.H. Miller, *Density-dependent feedback inhibition of oligodendrocyte precursor expansion.* J Neurosci, 1996. **16**(21): p. 6886-95.
27. Kang, S.H., et al., *NG2+ CNS glial progenitors remain committed to the oligodendrocyte lineage in postnatal life and following neurodegeneration.* Neuron, 2010. **68**(4): p. 668-81.
28. Kuhlmann, T., et al., *An updated histological classification system for multiple sclerosis lesions.* Acta Neuropathol, 2017. **133**(1): p. 13-24.
29. Lucchinetti, C., et al., *Heterogeneity of multiple sclerosis lesions: implications for the pathogenesis of demyelination.* Ann Neurol, 2000. **47**(6): p. 707-17.
30. Lazibat, I., M. Rubinić Majdak, and S. Županić, *Multiple Sclerosis: New Aspects of Immunopathogenesis.* Acta Clin Croat, 2018. **57**(2): p. 352-361.
31. Hohlfeld, R., et al., *The role of autoimmune T lymphocytes in the pathogenesis of multiple sclerosis.* Neurology, 1995. **45**(6 Suppl 6): p. S33-8.
32. Jurewicz, A., W.E. Biddison, and J.P. Antel, *MHC class I-restricted lysis of human oligodendrocytes by myelin basic protein peptide-specific CD8 T lymphocytes.* J Immunol, 1998. **160**(6): p. 3056-9.
33. Gharibi, T., et al., *The role of B cells in the immunopathogenesis of multiple sclerosis.* Immunology, 2020.
34. Ferguson, B., et al., *Axonal damage in acute multiple sclerosis lesions.* Brain, 1997. **120 (Pt 3)**: p. 393-9.
35. Bitsch, A., et al., *Acute axonal injury in multiple sclerosis. Correlation with demyelination and inflammation.* Brain, 2000. **123 (Pt 6)**: p. 1174-83.
36. Goldberg, J., et al., *Anatomical Distribution of Cuprizone-Induced Lesions in C57BL6 Mice.* J Mol Neurosci, 2015. **57**(2): p. 166-75.
37. Scheld, M., et al., *Neurodegeneration Triggers Peripheral Immune Cell Recruitment into the Forebrain.* J Neurosci, 2016. **36**(4): p. 1410-5.
38. Clementi, E., et al., *Persistent inhibition of cell respiration by nitric oxide: crucial role of S-nitrosylation of mitochondrial complex I and protective action of glutathione.* Proc Natl Acad Sci U S A, 1998. **95**(13): p. 7631-6.
39. Mahad, D., et al., *Mitochondrial defects in acute multiple sclerosis lesions.* Brain, 2008. **131**(Pt 7): p. 1722-35.
40. Linnane, A.W., et al., *Mitochondrial DNA mutations as an important contributor to ageing and degenerative diseases.* Lancet, 1989. **1**(8639): p. 642-5.
41. Hollensworth, S.B., et al., *Glial cell type-specific responses to menadione-induced oxidative stress.* Free Radic Biol Med, 2000. **28**(8): p. 1161-74.
42. Scheld, M., et al., *Mitochondrial Impairment in Oligodendroglial Cells Induces Cytokine Expression and Signaling.* J Mol Neurosci, 2019. **67**(2): p. 265-275.
43. Barnett, M.H. and J.W. Prineas, *Relapsing and remitting multiple sclerosis: pathology of the newly forming lesion.* Ann Neurol, 2004. **55**(4): p. 458-68.
44. Patrikios, P., et al., *Remyelination is extensive in a subset of multiple sclerosis patients.* Brain, 2006. **129**(Pt 12): p. 3165-72.
45. Nyamoya, S., et al., *G-Protein-Coupled Receptor Gpr17 Expression in Two Multiple Sclerosis Remyelination Models.* Mol Neurobiol, 2019. **56**(2): p. 1109-1123.

46. Ou, Z., et al., *Olig2-Targeted G-Protein-Coupled Receptor Gpr17 Regulates Oligodendrocyte Survival in Response to Lysolecithin-Induced Demyelination.* J Neurosci, 2016. **36**(41): p. 10560-10573.
47. Simon, K., et al., *The Orphan G Protein-coupled Receptor GPR17 Negatively Regulates Oligodendrocyte Differentiation via Gαi/o and Its Downstream Effector Molecules.* J Biol Chem, 2016. **291**(2): p. 705-18.
48. Fumagalli, M., et al., *Phenotypic changes, signaling pathway, and functional correlates of GPR17-expressing neural precursor cells during oligodendrocyte differentiation.* J Biol Chem, 2011. **286**(12): p. 10593-604.
49. Kipp, M., et al., *The cuprizone animal model: new insights into an old story.* Acta Neuropathol, 2009. **118**(6): p. 723-36.
50. Hall, S.M. and N.A. Gregson, *The in vivo and ultrastructural effects of injection of lysophosphatidyl choline into myelinated peripheral nerve fibres of the adult mouse.* J Cell Sci, 1971. **9**(3): p. 769-89.
51. Smith, R., *1H-nuclear magnetic resonance study of the association of the basic protein of central nervous system myelin with lysophosphatidylcholine.* Biophys Chem, 1982. **16**(4): p. 347-54.
52. Huang, J.K., et al., *Retinoid X receptor gamma signaling accelerates CNS remyelination.* Nat Neurosci, 2011. **14**(1): p. 45-53.
53. Kipp, M., *Remyelination strategies in multiple sclerosis: a critical reflection.* Expert Rev Neurother, 2016. **16**(1): p. 1-3.
54. Kipp, M., et al., *Experimental in vivo and in vitro models of multiple sclerosis: EAE and beyond.* Mult Scler Relat Disord, 2012. **1**(1): p. 15-28.
55. Herring, N.R. and C. Konradi, *Myelin, copper, and the cuprizone model of schizophrenia.* Front Biosci (Schol Ed), 2011. **3**: p. 23-40.
56. Taylor, L.C., W. Gilmore, and G.K. Matsushima, *SJL mice exposed to cuprizone intoxication reveal strain and gender pattern differences in demyelination.* Brain Pathol, 2009. **19**(3): p. 467-79.
57. Moore, S., et al., *Sex chromosome complement influences functional callosal myelination.* Neuroscience, 2013. **245**: p. 166-78.
58. Patel, R., et al., *Attenuation of corpus callosum axon myelination and remyelination in the absence of circulating sex hormones.* Brain Pathol, 2013. **23**(4): p. 462-75.
59. Leopold, P., C. Schmitz, and M. Kipp, *Animal Weight Is an Important Variable for Reliable Cuprizone-Induced Demyelination.* J Mol Neurosci, 2019. **68**(4): p. 522-528.

9. Danksagung

Allen voran möchte ich meinem Doktorvater Prof. Dr. med. Dr. rer. nat Markus Kipp für die exzellente Betreuung, das Heranführen an die wissenschaftliche Arbeitsweise, die freundschaftliche Unterstützung und die stete Ansprechbarkeit bei jeder noch so kleinen Problematik danken. Seine intensive wissenschaftliche Betreuung hat die vorliegende Dissertation und die zugrundeliegenden Publikationen überhaupt ermöglicht.

Darüber hinaus danke ich allen Mitarbeiterinnen und Mitarbeitern der Anatomischen Anstalt der Ludwig-Maximilians-Universität München, die zum Erfolg meiner Doktorarbeit beigetragen haben. Besonders hervorheben möchte ich dabei Sarah Wübbel, Astrid Baltruschat, Beate Aschauer und Sabine Tost und ihnen für ihre exzellente methodische und technische Assistenz sowie hervorragende Unterstützung bei der Durchführung der Experimente danken.

Mein Dank gilt auch allen Ko-Autoren, die an der Erstellung und Veröffentlichung der Arbeit mitgewirkt haben.

Besonderer Dank gilt meiner Doktorandengruppe für die fachliche, freundschaftliche, motivierende und lustige Zusammenarbeit bis spät abends sowie an Wochenend- und Feiertagen. Ich bin bis heute dankbar für die Freundschaften, die daraus entstanden sind. Meiner Mitbewohnerin, Mit-Doktorandin und „Partnerin-in-Crime seit Studium Tag 1“ Caro möchte ich noch einmal besonders für die allzeitige Diskussionsbereitschaft und unendlich langen Flurgespräche danken.

Für kreativen Input bei der Niederschrift und das Korrekturlesen danke ich besonders meiner Mutter und meiner Tante Petra.

Mein tiefer Dank gilt an dieser Stelle auch meinen Eltern, für ihre bedingungslose Unterstützung und Ermutigung in allen Lebenslagen sowie das Ermöglichen des Studiums, und meinen beiden Schwestern, durch die ich immer zwei Mitstreiterinnen an meiner Seite habe.

Ganz besonders möchte ich mich auch noch bei meinem Freund Philip bedanken, der mich über den gesamten Weg der Doktorarbeit begleitet hat und stets ein offenes Ohr und unterstützende Worte für mich bereithielt.